Manuscript for *Revista Mexicana de Astronomía y Astrofísica* (2007)

OPTICAL SPECTROSCOPIC ATLAS OF THE MOJAVE/2CM AGN SAMPLE[1]

Janet Torrealba[2,3], Vahram Chavushyan[2], Irene Cruz-González[3], Tigran G. Arshakian[4,5], Emanuele Bertone[2], Daniel Rosa-González[2]

Draft version: September 13, 2011

RESUMEN

Presentamos un atlas espectroscópico óptico de resolución intermedia (8–15 Å) para 123 núcleos activos de galaxias compactos con la presencia de chorros superlumínicos, tomados de la muestra limitada en densidad de flujo a 15 GHz MOJAVE/2cm. Es la primera vez que se presentan los parámetros espectroscópicos y fotométricos para una muestra tan grande de este tipo de AGN. El atlas incluye los parámetros espectrales para las líneas de emisión Hβ, [O III]λ5007, Mg IIλ2798 y/ó C IVλ1549, junto con los datos para la emisión del continuo correspondiente. Se presentan además las luminosidades y el ancho equivalente del Fe II UV/óptico. Contiene también la información fotométrica homogénea en la banda B para 242 fuentes de la muestra, con un pico en la distribución de B_J=18.0 y un intervalo en magnitud de $11.1 \leq B_J \leq 23.7$.

ABSTRACT

We present an optical spectroscopic atlas at intermediate resolution (8–15 Å) for 123 core-dominated radio-loud active galactic nuclei with relativistic jets, drawn from the MOJAVE/2cm sample at 15 GHz. It is the first time that spectroscopic and photometric parameters for a large sample of such type of AGN are presented. The atlas includes spectral parameters for the emission lines Hβ, [O III]λ5007, Mg IIλ2798 and/or C IVλ1549 and corresponding data for the continuum, as well as the luminosities and equivalent widths of the Fe II UV/optical. It also contains the homogeneous photometric information in the B-band for 242 sources of the sample, with a distribution peak at B_J=18.0 and a magnitude interval of $11.1 \leq B_J \leq 23.7$.

Key Words: atlases — galaxies: active — galaxies: nuclei — quasars: emission lines — techniques: spectroscopic

1. INTRODUCTION

In the current paradigm of active galactic nuclei (AGN), the large amount of energy released by the AGN is generated in the very small region, the central

[1]These data were acquired at Observatorio Astronómico Nacional in San Pedro Mártir (OAN–SPM), México and at Observatorio Astronómico Guillermo Haro, in Cananea, Sonora (OAGH)

[2]Instituto Nacional de Astrofísica, Óptica y Electrónica, México

[3]Instituto de Astronomía, UNAM, México

[4]Max-Planck/Institut für Radioastronomie, Bonn, Germany

[5]Byurakan Astrophysical Observatory, Byurakan 378433, Armenia and Isaac Newton Institute of Chile, Armenian Branch

engine, which is thought to be powered by accretion of matter onto a central black hole. This active central engine also ejects bipolar, highly collimated, relativistic outflows (jets). AGN in which one of the jets is oriented towards the line of sight is strongly beamed due to relativistic effects. This type of sources poses several fundamental questions such as: how the central engine is related to the pc-scale jets; what is the contribution of the jet emission to the total continuum emission and line emission; how are related the continuum emission region, broad/narrow emission-line region with different properties of the relativistic jet. Despite all the advances in AGN research, a global analysis of the physics involved at all spatial scales, from sub-parsec to kpc, is needed to tackle above issues.

Recently, Arshakian et al. (2008, 2010a) and León-Tavares et al. (2010), using the long-term optical spectral and radio (VLBI) monitoring data of radio galaxies 3C 390.3 and 3C 120 found a link between the variable optical emission and the kinematics of the sub-parsec-scale jet. They have been able to localize the region of a variable optical emission in the innermost sub-pc scale region of the jet, and showed that very long-term variations ($\sim$ 10 yr) of optical continuum emission are correlated with the radio emission from the base of the jet located just above the disk, while the optical long-term variations (1–2 yr) follow the radio flares from the stationary component in the jet with a time delay of about one yr. Using the flux-limited complete sample of core-dominated AGN (MOJAVE-1; Lister et al. 2009), Arshakian et al. (2010b) found interesting correlations among properties of parsec-scale jets, using the photometric data presented in this atlas. They reported a significant positive correlation between optical nuclear emission and total radio emission at 15 GHz for 99 quasars. Radio emission originates in the unresolved core, at milliarcsecond scales suggesting that both radio and optical emission are beamed and originated in the innermost part of the sub-parsec-scale jet in quasars. For BL Lacs, the optical continuum emission correlates with the radio emission of the jet. These results are confirmed for a larger sample of 233 core-dominated AGN (Torrealba et al. 2011).

Furthermore, spectroscopic parameters of the broad- and narrow-line profiles provide a direct clue about the physics, kinematics, and structure of the central engine of AGN. Diverse studies have shown the existence of an anticorrelation between the prominence of the radio nucleus and the width of broad emission line, giving a clue on the gas distribution in the broad line region (BLR) in these sources (Hα, Hβ, Mg II, and others lines; Hough et al. 2002; Vestergaard et al. 2000; Wills & Browne 1986). The results of Rokaki et al. (2003) confirmed the correlation between the jet viewing angles and the broad emission line equivalent widths of 19 superluminal quasars, which suggests a flattened structure for the line-emitting material.

Motivation of the present paper is to perform a robust statistical analysis and to study in detail the physical link between the diverse emission regions in radio-loud AGN from sub-pc to kpc scales. For this purpose it is necessary to compile a well defined sample of compact AGN with superluminal jets

and a collection of good quality spectral parameters (signal–to–noise ~ 30). Here, we gathered the spectroscopic and photometric information for a specific subsample of 250 compact AGN (selected from the MOJAVE sample) for which the jet parameters are well characterized (Kovalev et al. 2005).

We present an optical spectroscopic atlas of 123 AGN that represent the $\sim$50% of the total sample, supplemented with the photometric information for 97% of the same sample (242 sources). The contents of the paper are as follows: the sample is described in § 2, followed by the photometric data and calibration for estimating the optical luminosities at 5100 Å (§ 3); details of optical spectroscopic observations are presented in § 4, followed by data reduction and calibration procedures in § 5; the detailed procedure to extract the principal parameters of the continuum emission and various emission lines (Hβ, [O III]λ5007, Mg IIλ2798, C IVλ1549, and Fe II UV/optical) are described in § 6, followed by the results in § 7, and finally, the appendices contain the general properties of the sample in A, spectral atlas in B, and emission line parameters and continuum emission in C.

Throughout the paper a flat cosmology model is used with $\Omega_m = 0.3$ ($\Omega_\Lambda + \Omega_m = 1$) and $H_0 = 70$ km s^{-1} Mpc^{-1}.

2. MOJAVE/2CM AGN SAMPLE

We use the sample of 250 compact extragalactic sources compiled by Kovalev et al. (2005). The sources were observed with the Very Large Baseline Array (VLBA) at 2 cm (15 GHz) and present radio jets on parsec scales. The sample is composed from: *i)* the flux-density-limited complete sample MOJAVE-1 of 135 sources (Monitoring of Jets in AGN with VLBA Experiments; Lister et al. 2009), hereon M1; *ii)* the extension MOJAVE-2 of 53 AGN with special characteristics (e.g. high luminosities, special kinematics, γ-ray sources); and *iii)* 62 sources from the VLBA 2 cm monitoring survey (Kellermann et al. 1998, 2004; Zensus et al. 2002). We refer to this sample as MOJAVE/2cm.

Since 1994, the VLBA 2 cm survey and MOJAVE program have monitored compact radio sources to study their jets structure with unprecedented resolution and sensitivity (see Lister et al. 2009, and references within). Most of the sources in our sample have flat radio spectra ($\alpha > -0.5$, $F \sim \nu^{+\alpha}$, for $\nu > 500$ MHz; Kovalev et al. 1999, 2000), and their total flux density[6] at 2 cm is greater than 1.5 Jy for sources with $\delta > 0^\circ$ and > 2 Jy for sources with $-20^\circ < \delta < 0^\circ$.

The summary of spectroscopic classification from Véron-Cetty & Véron (2003) AGN catalog is presented in Table 1. The full sample consists of 188 quasars, 36 BL Lacs, 20 radio galaxies (RG), and 6 sources with no optical identification (see Table 6 Appendix A). Among quasars there are 49 high polarized quasars (optical polarization $P > 3$%, HPRQ), 22 low polarized

[6]Total flux density was obtained in the period 1994–2003, often originally estimated by extrapolation from lower frequency data (Kovalev et al. 2005).

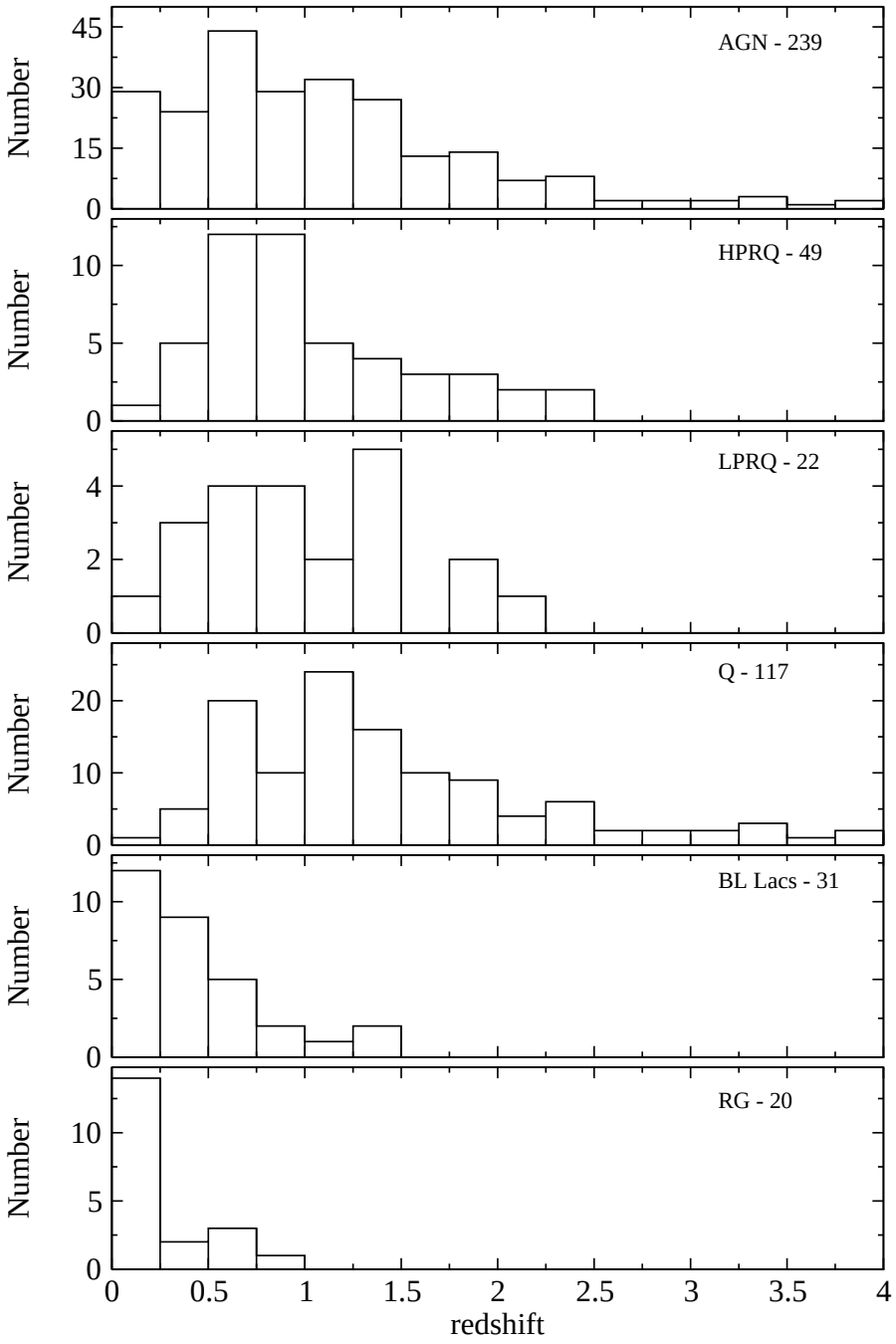

Fig. 1. Distribution of redshifts of the MOJAVE/2cm AGN is shown in the top panel. Other panels show the distributions of redshifts for different spectral types of AGN.

TABLE 1

SPECTROSCOPIC CLASSIFICATION OF THE MOJAVE/2CM AGN

Sample	#	Quasars	BL Lac	RG	No ID
MOJAVE-1[a]	135	101	22	8	4
MOJAVE-2[b]	53	35	10	8	···
2cm[c]	62	52	4	4	2
MOJAVE/2cm	250	188	36	20	6

[a]M1: Lister & Homan (2005), redshift $0.004 \leq z \leq 3.408$ and magnitude $11.16 \leq B \leq 22.10$.

[b]M2: Currently monitored (`http://www.physics.purdue.edu/MOJAVE/`), redshift $0.017 \leq z \leq 3.280$ and magnitude $13.14 \leq B \leq 20.92$.

[c]2 cm: Kellermann et al. (1998); Zensus et al. (2002); Kellermann et al. (2004), redshift $0.055 \leq z \leq 3.787$ and magnitude $12.15 \leq B \leq 23.40$.

quasars ($P < 3\%$, LPRQ), and 117 quasars without optical polarimetry information (Q).

The distributions of redshifts of 239 MOJAVE/2cm AGN and individual types of AGN are shown in the different panels of Figure 1. The AGN redshift range is $0.004 \leq z \leq 3.8$ and the mean redshift is 1.1.

The apparent B-magnitude in the Johnson's photometric system, B_J, for 242 MOJAVE/2 cm sources is shown in Figure 2, where the dotted area shows sources with spectrophotometric data, which represents ∼50% of the sample. The remaining sources are too faint for spectroscopy with 2m-class telescopes. The peak of the distribution is at $B_J = 18.0$ and $11.1 \leq B_J \leq 23.7$.

3. OPTICAL LUMINOSITIES

In this work we estimate the optical luminosity at 5100Å (λL_{5100}) for 233 sources of MOJAVE/2cm compact radio sources drawn for the photometric data available for each AGN. We report as well the spectroscopical parameters of the continuum emission and diverse emission lines, measured directly from the data of 123 AGN of the same sample depending on the redshift of the source. The procedure to obtain λL_{5100} is described below, while the treatment of the spectroscopical data is explained in section § 6.

The luminosity at 5100Å is estimated using the following expression (e.g., Marziani et al. 2003b):

$$\lambda L_{5100} = 3.137 \times 10^{35-0.4(M_{\rm B}-A_{\rm B})}\,{\rm erg\,s^{-1}}, \quad (1)$$

where $A_{\rm B}$ is the galactic extinction in the B-band taken from the NASA Extragalactic Database, and $M_{\rm B}$ is the absolute magnitude given by Schmidt & Green (1983):

$$M_{\rm B} = B_J - 5\log d_L + 2.5\,(1+\alpha_{op})\,\log(1+z) + 5\,\log(h) - 42.386. \quad (2)$$

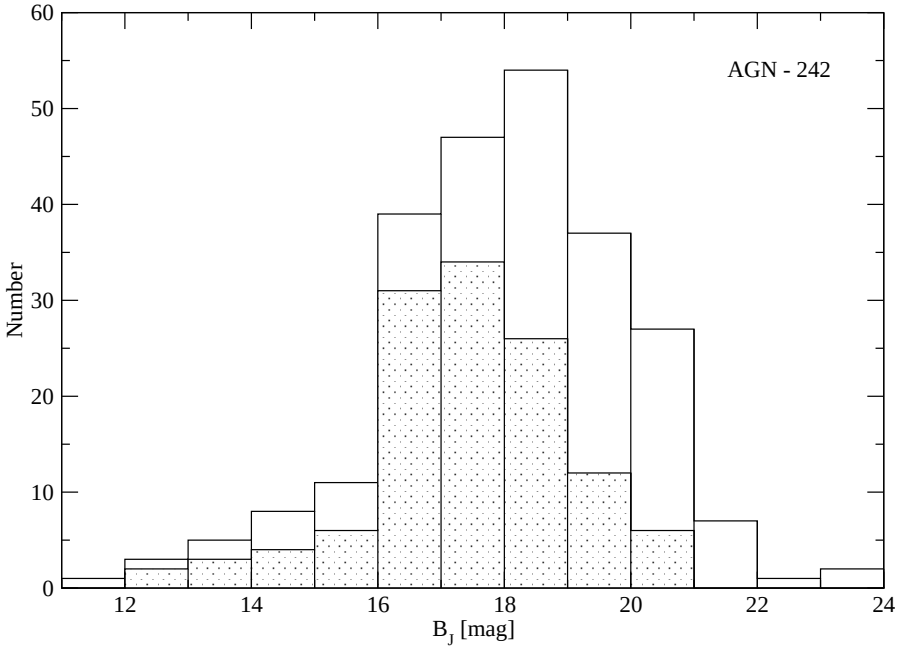

Fig. 2. Distribution of apparent B-magnitudes of the MOJAVE/2cm AGN. The dotted histogram represents the ∼50% of the sources that have spectrophotometric data.

In this equation $h = H_0/100\,\mathrm{km\,s^{-1}\,Mpc^{-1}} = 0.7$; the term $2.5\,(1+\alpha_{op})\,\log(1+z)$ reflects the effect of the redshift on measurements through a fixed color band. We adopted an optical spectral index $\alpha_{op} = -0.5$ ($S_\nu \propto \nu^\alpha$) typical value for radio-loud objects (see Table 2 Brotherton et al. 2001). Finally, z is the redshift, and d_L is the luminosity distance for the flat cosmology model given by

$$d_L = \frac{c}{H_0}(1+z)\left[\eta(1,\Omega_\mathrm{m}) - \eta\left(\frac{1}{1+z},\Omega_\mathrm{m}\right)\right], \qquad (3)$$

where Ω_m=0.3 and η is a function of z and Ω_m (see Pen 1999).

The details on the calculation of B_J and the procedure to correct by the host galaxy contribution is described in Arshakian et al. (2010b).

The distribution of λL_{5100} covers 5 orders of magnitude in luminosity with a range between $2 \times 10^{42}\,\mathrm{erg\,s^{-1}}$ and $1 \times 10^{47}\,\mathrm{erg\,s^{-1}}$, with an average value of $9 \times 10^{45}\,\mathrm{erg\,s^{-1}}$; as is shown in Figure 3 for the different AGN types in our sample. The radio galaxies are the sources with weaker luminosities as compared with the quasars and BL Lacs. The distributions of the optical nuclear luminosities for HPRQ and LPRQ show slightly different ranges: $\lambda L_{5100,\,\mathrm{HPRQ}} = (10^{43}-10^{46})\,\mathrm{erg\,s^{-1}}$ and $\lambda L_{5100,\,\mathrm{LPRQ}} = (10^{44}-10^{46})\,\mathrm{erg\,s^{-1}}$. The Kolmogorov-Smirnov test (KS) shows that the null hypothesis that these distributions are drawn for the same parent population cannot be rejected at a confidence level 93% ($P_{KS} = 0.072$), for M1 sample the confidence level is 81%, ($P_{KS} = 0.189$). It is well known that HPRQ fall within the group of

blazars and are known to exhibit a different behavior regarding LPRQ, and their differences cannot be explained with a model based solely on orientation effects. For example, Lister & Smith (2000) found that the cores of the LPRQ tend to be less luminous at 15 GHz than the HPRQ. Besides, they reported that the jet components in the LPRQ have magnetic fields parallel to the jet, while those of HPRQ are perpendicular to the flow of the jet. We agree that high– and –low polarized quasars are intrinsically different sources, but more observational data (polarization studies) are needed to understand the physical nature of the differences showed in these two types of quasars.

4. SPECTROSCOPIC OBSERVATIONS AND SUPPLEMENTARY DATA

Optical spectra of the bright fraction ($B < 18$) of AGN of the sample were obtained in several observing runs from 2003 to 2006 with two optical telescopes in Mexico: the 2.1m telescope of the Observatorio Astronómico Nacional in San Pedro Mártir, Baja California (OAN–SPM), and the 2.1m telescope of the Observatorio Astronómico Guillermo Haro, in Cananea, Sonora (OAGH). From these telescopes we obtained a total of 146 good quality spectra: 110 from OAN–SPM and 36 from OAGH.

The OAN–SPM spectra were obtained with a Boller & Chivens spectrograph, using a 2.5 $''$ slit, a CCD SITe3 (1024 $\times$ 1024 pixels of 24 μm$\times$ 24 μm), a plate scale of 40 $''$/mm), a 300 l/mm grating and blaze angle of 5°50′ for the 4000–8000 Å spectral region, obtaining an effective spectral resolution of $\sim$ 8–10Å.

The OAGH spectra were obtained with a Boller & Chivens spectrograph, using a 2.5 $''$ slit, a CCD Tektronix TK1024 (1024 $\times$ 1024 pixels of 24 μm $\times$ 24 μm) and a plate scale of 8.18 $''$/mm, a 150 l/mm grating and blaze angle of 3°00′ for the 4000–7100 Å spectral region, obtaining an effective spectral resolution of $\sim 10 - 15$ Å.

We also searched for spectroscopic data in the archives of the Sloan Digital Sky Survey (*SDSS*), the Hubble Space Telescope (*HST*), and in the AGN sample of Marziani et al. (2003a)[7], hereafter M03. The database was also supplemented by spectra kindly provided by C. R. Lawrence (Lawrence et al. 1996, hereafter L96). In total, we found 114 additional spectra: 23 from *SDSS*, 40 from *HST*, 36 from L96, and 15 from M03.

Overall, 260 spectra of 123 AGN were analyzed from both our spectroscopic observations and the supplementary data. From these 123 AGN, 73 sources belong to the flux-limited sample MOJAVE-1 (4 BL Lacs, 7 RG, 24 HPRQ, 17 LPRQ, and 21 Q). For this sub-sample we have a total of 104 spectra: 37 from OAN-SPM, 18 from OAGH, 17 from SDSS, 13 from HST, 10 from L96, and 9 from M03.

The typical integration times of our observations were 3600 s splitted in three exposures per source for an object with $B \sim 18$. The spectra for *HST*, *SDSS*, L96, and M03 involved typical total integration times of 1000 sec, 3800, 3100, and 10,000 sec, respectively.

[7] `http://web.pd.astro.it/marziani/data.html`

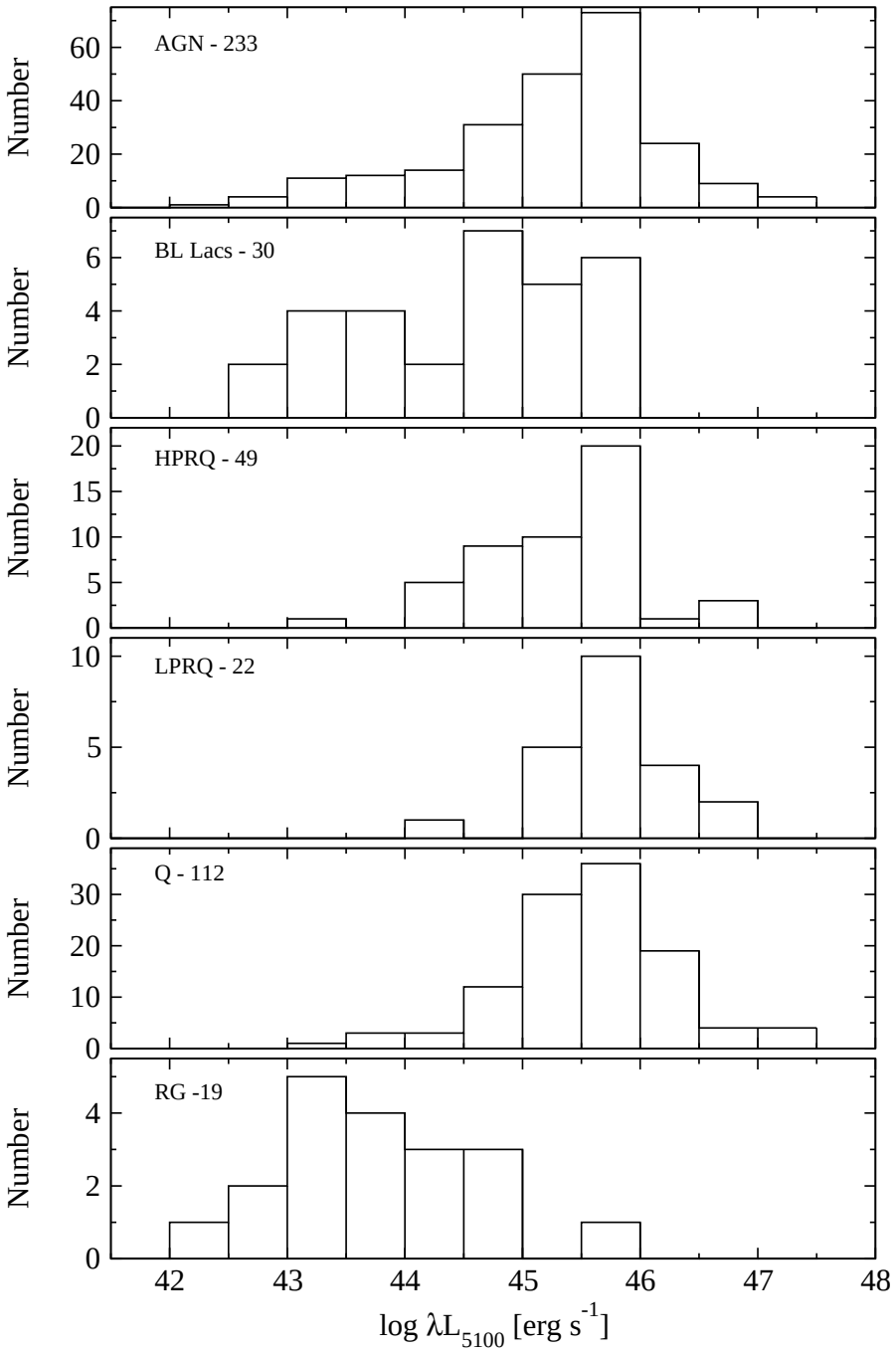

Fig. 3. The distribution of corrected photometric optical luminosities at 5100 Å for the sample of 233 AGN for the MOJAVE/2cm sample (top panel), 30 BL Lacs, 49 HPRQ, 22 LPRQ, 112 quasars, 19 radio galaxies, and 1 unidentified source.

TABLE 2

SYNOPSIS OF OPTICAL SPECTROSCOPY

Obs.	Tel. Apert.	Spectr.	Grating ($l\,mm^{-1}$)	Slit Width ($''$)	Spectr. Resol. (Å)	# spectra[a]
OAN/SPM	2.1m	B&Ch	300	2.5	8-10	110 (37)
OAGH	2.1m	B&Ch	150	2.5	10-15	36 (18)
SDSS	2.5m	MOS[b]	420	···	~ 3	23 (17)
HST	2.4m	FOS[c]	G270H	2.0	~ 2	40 (13)

[a]The numbers in parentheses refer to data acquired from the sample MOJAVE-1.

[b]MOS: multi-object fiber spectrographs with two channels red (420 $l\,mm^{-1}$) and blue (640 $l\,mm^{-1}$). For specifications see `http://www.jhu.edu/~sdss/Spectrographs/OptLayout.html`.

[c]Spectral resolution for the *HST-FOS* data varies depending on the grating and slit width: e.g. G270H– $0.25\times2.0''$–1.92 Å, G400H –$4.3''$–2.88Å.

Table 2 summarizes the instrumental setup and spectroscopic characteristics of the different sets of optical spectra. Data is organized as follows: Col. (1) is the observing site, Col. (2) is the telescope aperture, Col. (3) is the spectrograph, Col. (4) is the dispersion in $Å\,mm^{-1}$, Col. (5) is the slit width in $''$, Col. (6) is the spectral resolution in Å at FWHM measured on the instrumental profile, and Col. (7) is the number of spectra. Observational details of the spectra obtained from L96 are presented in their Tables 1 and 2, and from M03 is presented in their Table 1. The data of L96 has a spectral resolution in the range between 6–18 Å, and for the data of M03 the spectral resolution is in the range between 3–8 Å.

5. DATA REDUCTION AND CALIBRATION

The data reduction was performed with the standard procedure using IRAF[8] routines for a long-slit spectroscopy, i.e., bias subtraction, flat-fielding, cosmic-ray removal, and sky subtraction, to produce the final spectra. We also observed standard stars for flux calibration. Wavelength calibration was achieved via observations of HeAr lamp at OAGH and HeAr/CuHeNeAr lamp at OAN–SPM. The arc spectra was obtained after an exposure (if single) or between exposures (if two or more consecutive exposures were taken), with the telescope still pointing towards the target. This calibration was accomplished by fitting a polynomial of suitable order to the pixel wavelength correlation with an uncertainty of ~ 0.5 Å rms for all cases; this was checked using the

[8]IRAF is the Image Reduction and Analysis Facility made available to the astronomical community by the National Optical Astronomy Observatories, which are operated by AURA, Inc., under contract with the U.S. National Science Foundation. It is available at `http://iraf.noao.edu/`

positions of background night sky lines. Flux calibration was performed using the cataloged spectrophotometric standards stars (Massey et al. 1988; Oke 1990). Usually, one or two stars at similar airmass of the principal target were observed on the same observing night. Atmospheric extinction correction was applied using the extinction curve for OAN–SPM[9] and OAGH[10]. Objects with more than one observation had their spectra stacked together to increase the signal-to-noise ratio (S/N). The average S/N ratio achieved was approximately 20, 30, and 10 in the continuum near 5100 Å, 3000 Å, and 1350 Å, respectively.

6. ANALYSIS OF SPECTRA

The general data processing of spectra involved several steps. Once the spectra were flux calibrated, they were shifted to the rest frame of the source with the available redshift data. Then the iron contribution was subtracted and the local continuum emission was fitted with a power law. Finally, the continuum and line parameters were measured. Each of these procedures are described in more detail in the following sections.

6.1. *Continuum and iron contamination subtraction*

Since we are interested in studying the profiles of the emission lines (Hβ, Mg IIλ2798, and C IVλ1549) it is crucial to subtract the Fe II emission in both optical and ultraviolet spectral regions.

First, the continuum emission of the rest frame spectra was fitted by a power-law ($a\,\lambda^b + c$) in appropriately selected windows and subtracted using the Levenberg-Marquardt[11] least-squares minimal routine. Then, the resulting spectra is compared with the Fe II templates in selected spectral regions, which can be modified for the corresponding observed spectral resolution and broadening. The best fit of iron emission is subtracted from the spectra.

The following Fe II templates of the NLS1 I Zw 1 galaxy ($z = 0.0611$; FWHM of $\simeq 900$ km s^{-1}) were used: (a) the template of Véron-Cetty et al. (2004) based on spectra from the 4.2 m William Hershel and the 3.9 m Anglo-Australian telescopes for the optical band (from 3575–7530 Å); and (b) the template of Vestergaard & Wilkes (2001), based on spectra from the *HST-FOS*, for the UV-band (from 1250–3090 Å). These are the more accurate templates available in the literature. The intrinsic narrow lines of this source and its rich iron spectrum make the templates particularly suitable for use with AGN spectra.

Possible continuum windows for each iron region of interest are presented in Table 3. An example of the iron subtraction is illustrated in Figure 4 for two sources in the Hβ and Mg II regions.

[9] Determined by Schuster & Parrao (2001); available at `http://www.astrossp.unam.mx/indexspm.html`

[10] `http://www.inaoep.mx/~astrofi/cananea/oagh-sky.html#Extinction`

[11] We used the IDL routine MPFIT from `http://cow.physics.wisc.edu/~craigm/idl/fitting.html`

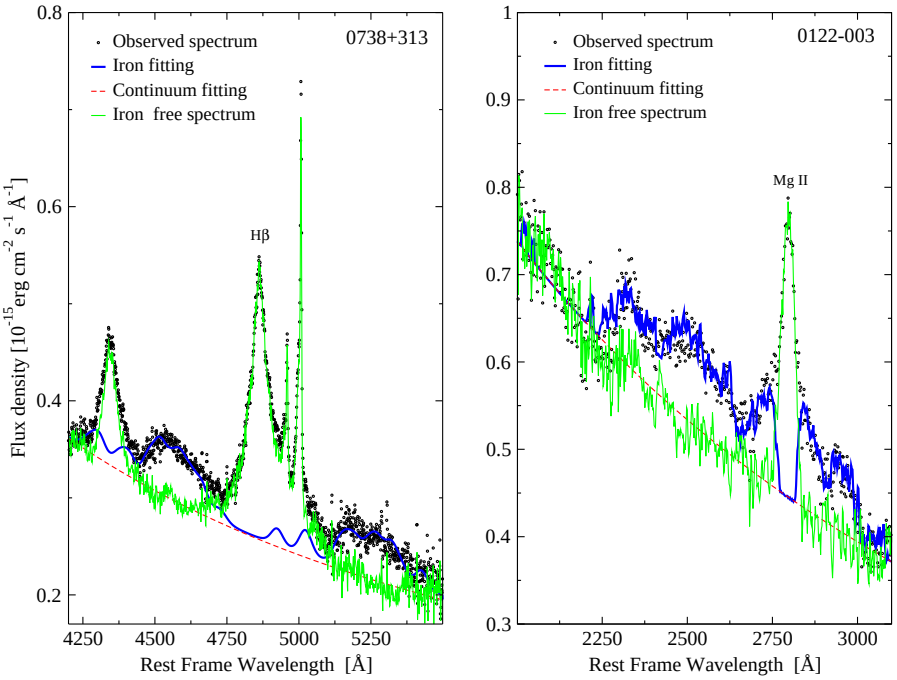

Fig. 4. Examples of the subtraction of Fe II emission: *left panel* in the Hβ region for quasar 0738+313 and *right panel* in the Mg II region for quasar 0122−003. It shows the observed spectrum in rest frame (circles); the Fe II fitting (*blue solid line*); the power-law continuum fitting (*red dashed line)*; the spectrum after Fe II subtraction (*green solid line*). The Mg II emission line profile drastically changes after removing the iron contribution.

TABLE 3

SELECTED CONTINUUM AND FE II WINDOWS

	Rest wavelength interval (Å)	
Emission Line	Continuum	Fe II
Hβ[a]	4210–4230	4400–4750
λ4861	5080–5100	5150–5500
Mg II[a]	2220–2230	2300–2650
λ2798	3010–3040	2900–3090
C IV[b]	1265–1290	···
λ1549	1340–1375	···
	1425–1470	···
	1680–1705	···
	1950–2050	···

[a]Continuum windows from Kuraszkiewicz et al. (2002).

[b]Continuum windows from Vestergaard & Peterson (2006).

6.2. *Continuum flux*

We obtained the mean value of the continuum emission flux density f_λ centered at the given wavelength in an interval of ± 50 Å from the iron free spectrum of each AGN. In this manner, we estimated the flux density f_{5100} in the interval 5050 Å$< \lambda <$5150 Å, f_{3000} in 2950 Å$< \lambda <$3050 Å, and f_{1350} in 1300 Å$< \lambda <$1400 Å. The associated error in the continuum flux density is $\sim$10 % and depends on the S/N ratio of individual spectrum. In few particular cases, where the spectral interval was not enough to get a mean value, we estimated f_λ by using the power-law $f_\lambda = a\,\lambda^b + c$ that fits the continuum as described in § 6.1 above.

6.3. *Emission-line parameters*

The emission lines were fitted with Gaussian profiles (Veron et al. 1980), assuming a broad and narrow components, which characterize the kinematics of the broad and narrow line regions (BLR and NLR, respectively). The minimal least-square fitting provides the central position of the Gaussian λ_c, full width at half maximum (FWHM), equivalent width (EW), and line flux.

Four Gaussian components were used for the spectral region of Hβ: two for Hβ line (narrow and broad) and two for forbidden lines [O III] $\lambda\lambda$4959, 5007. The narrow component (NC) of Hβ (H$\beta_{\rm NC}$) was modelled and subtracted using the Gaussian profile fitted to the [O III] line, assuming that the [O III] line ratio [O III]λ5007/[O III]λ4959 is 2.96 (Osterbrock 1989). In this

way, the H$\beta_{\rm NC}$ FWHM was determined by the [O III] FWHM. The remaining parameters were set free in the fitting. In particular cases, where the narrow component position was not evident, it was fixed to the central wavelength of the Hβ line. The fitting was done in the spectral interval 4700–5200 Å.

For the Mg II and C IV lines, the restriction used was that the narrow component FWHM $\leq 2000\,{\rm km\ s^{-1}}$. This condition was used by McLure & Dunlop (2004), because there is no narrow line in the spectral range that could be modelled to subtract the narrow component from the total line profile. As in Hβ, if necessary, the position of the Gaussian NC was fixed in the fitting. Fitting of the Mg II and C IV lines were performed in the spectral ranges 2600–3000 Å and 1450–1650 Å, respectively. The local continuum in each case was also fitted in the spectral ranges previously mentioned.

The obtained residuals in the fitting compared to the observed spectra were always less than 5 % in the three subsamples. In Figures 5, 6, and 7 an example of the fitting is shown for the lines Hβ, Mg II, and C IV, respectively.

Once the FWHM of the lines was obtained, an instrumental resolution correction was applied by means of the equation:

$$\mathrm{FWHM}_{corrected} = (\mathrm{FWHM}^2_{observed} - \mathrm{FWHM}^2_{instrumental})^{1/2} \qquad (4)$$

The mean value of the instrumental resolution for the spectra obtained in OAN-SPM and OAGH was ~ 8.5 Å and ~ 15 Å, respectively. For the *SDSS* spectra a mean value of ~ 3 Å was used for the instrumental resolution, and 2 Å was used for the *HST-FOS* spectra. The instrumental resolution for the spectra of L96 was obtained from their Table 2, and for M03 spectra it was extracted from their Table 1.

6.4. *Continuum and emission line luminosities.*

Once we had the continuum and emission line fluxes, the corresponding luminosities were calculated. First, the rest frame flux f_λ was corrected for local reddening, applying the following expression:

$$f_c = f_\lambda\, 10^{(0.4\, A_V\, K_\lambda)}, \qquad (5)$$

where f_c is the reddening corrected flux represented by a density flux in the case of continuum emission and integrated flux in the case of line emission. The reddening A_V was calculated assuming A_V=A_B/1.32, where A_B is the B-band extinction and K_λ is estimated from the Galaxy extinction curve of Howarth (1983). The A_B values were obtained from the NED[12], where dust extinction maps of Schlegel et al. (1998) are used, which are based on the infrared difuse emission data from IRAS/DIRBE. The typical extinction for the Hβ, Mg II, and C IV subsamples is 0.566 mag, 0.342 mag, and 0.547 mag, respectively. The values of A_B used are given in Table 6 for each AGN.

The luminosity was calculated for the corrected fluxes with the usual relation $L = 4\pi\, {d_L}^2 f_c$, where d_L is the luminosity distance of the object given by equation (3).

[12]NASA/IPAC Extragalactic Database.

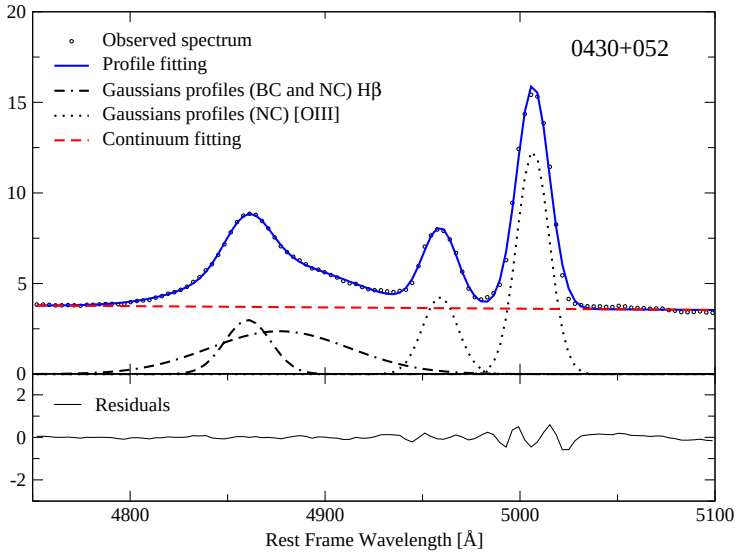

Fig. 5. Fitting of the Hβ λ4861 and [O III] lines profiles of the AGN 0430+052. The abscissa corresponds to the rest wavelength in Å while the ordinate is the flux density in units of 10^{-15} erg s^{-1} cm^{-2} Å^{-1}. The upper panel shows the observed spectrum (*empty circles*), the profile fitting (*solid line*) comprises by the fitting for 4 Gaussians: 2 for Hβ (*dotted lines and points*) and 2 for [O III] $\lambda\lambda$4959,5007 (*dotted lines*), where the intensity ratio was fixed to 2.96; and the power-law local continuum fitting (*dashed line*). The width of the narrow component (NC) of Hβ was fixed using the line [O III] λ5007. In the lower panel are shown the residuals of the fit, with a mean value of 1.9 % compared to the observed spectra.

6.5. *Measurement of Fe II emission*

The identification of iron in the spectra of AGN dates from 40 years ago (e.g., Greenstein & Schmidt 1964). Joly (1987) studied the physical conditions required to explain the observed Fe II in AGN spectra. Iron emission measurements in the optical region have shown that this emission (Fe II$_{opt}$) is a distinctive parameter to separate type I from type II AGN (Marziani et al. 2003a). In the ultraviolet Wills et al. (1980) showed spectra of intermediate redshift quasars ($z \sim 1$) with prominent Fe II emission.

The Fe II emission lines can be split into various wavelength bands. In the ultraviolet approximately 2000–3000 Å and 3000–3400 Å; and in the optical ∼4500–4700 Å and ∼5000–5400 Å (e.g. Osterbrock 1977; Phillips 1978; Joly 1987).

In the optical, the strongest feature, designated as Fe II λ4570 arises from lines in the range 4470–4670 Å (see Osterbrock 1977; Phillips 1978; Joly 1987), while other lines contribute to the prominent Fe II bands denoted as

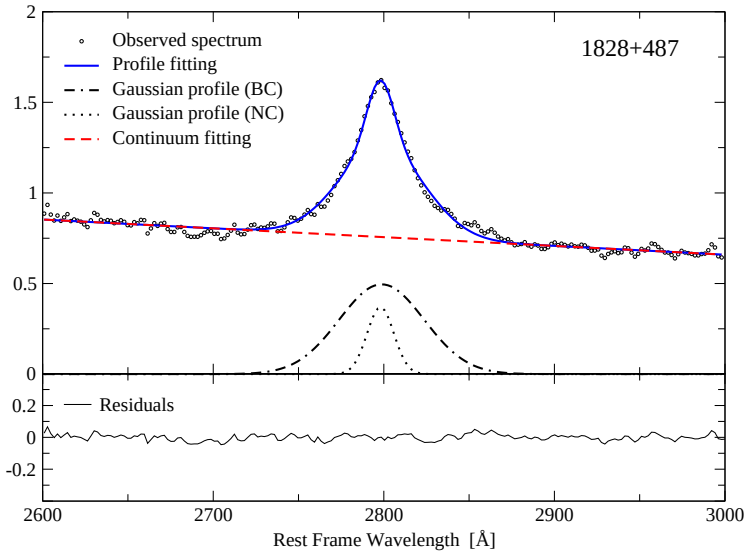

Fig. 6. Fitting of the Mg IIλ2798 line profile for the AGN 1828+487. The abscissa corresponds to the rest wavelength in Å while the ordinate is the flux density in units of 10^{-15} erg s^{-1} cm^{-2} Å^{-1}. The upper panel shows the profile fitting (*solid line*) comprises by the fitting with 2 Gaussians curves and the power-law local continuum emission (*dashed line*). The Gaussian functions represent the broad component (BC, *dotted line and points*) and the narrow component (NC, *dotted line*) of the line. The width of the NC was restricted to a FWHM < 2000 km s^{-1}. In the lower panel are shown the residuals of the fit, with a mean value of 2.4 % compared to the observed spectra.

Fe II λ5190 and Fe II λ5320. The AGN redshifts and the instrumental setup used in our sample favours the detection of the Fe II λ4570 multiplet, which is extensively studied in the literature (e.g. Collin & Joly 2000; Joly 1987; Marziani et al. 2003a; Zhang et al. 2006, 2007)

The equivalent width of the Fe II λ4570 emission, denoted as EW(Fe II λ4570), was calculated via the usual definition EW(Fe II λ4570)= f_{FeII}/f_c, where f_{FeII} is the Fe II total flux in the spectral range 4450–4600 Å, and f_c is the continuum flux intensity measured in the interval 4520–4620 Å. The mean value for the EW(Fe II λ4570) is 18.2 Å with a standard deviation of 16.6 Å (c.f. Table 5).

In the ultraviolet at $\lambda < 3000$ Å, the different regions involve the wings of the Mg II λ2798 emission line. The blue part, in the range 2100–2800 Å, is formed by Fe II λ2100, Fe II λ2500, and Fe II λ2750 (Grandi 1981) and is denoted as Fe II λ2490. The first spectral region is also known as Fe II λ2050, the second corresponds to the range 2300–2600 Å, and the third spectral region

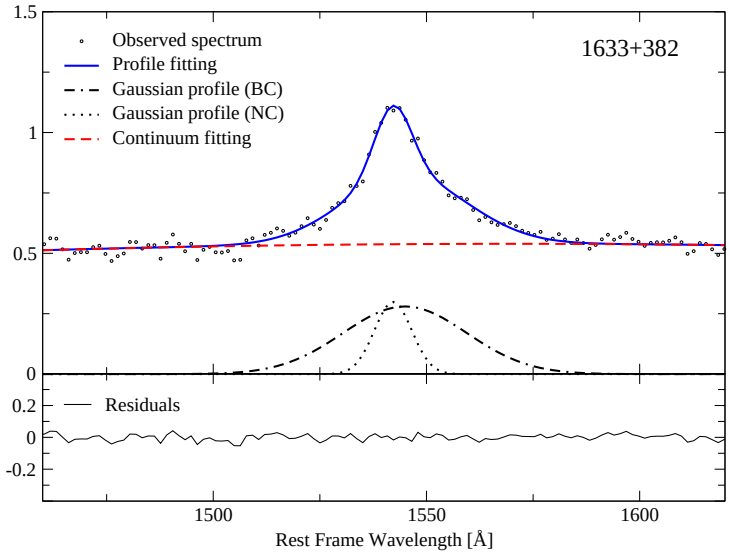

Fig. 7. Fitting of the C IV λ1549 profile for the AGN 1633+382. The symbols are the same as in Figure 5. Also the restriction for the NC was applied to the fit. In the lower panel, the residuals of the fit are shown, with a mean value of 3.4 % compared to the observed spectra.

was named by Wills et al. (1980), and partially includes the Mg II λ2798 line. The red part is called Fe II λ2950 and Fe II λ3200. The instrumental setup used and the AGN redshifts limit our study to the blue part of the spectrum. The same procedure used for deriving the Fe II λ4570 parameters was used to estimated the Fe II λ2490 parameters. The mean value estimated for EW(Fe II λ2490) was 54.2 Å with a standard deviation of 25.8 Å.

7. RESULTS

7.1. *Photometric Data for MOJAVE/2cm AGN Sample*

The MOJAVE/2cm sample of 250 AGN is presented in the Appendix A, together with the homogeneous photometric information at the B-band. Table 6 is organized as follows: Col. (1) is the source name, Col. (2)–(3) are the J2000.0 coordinates, Col. (4) is the spectroscopic classification from Véron-Cetty & Véron (2003) (B = BL Lac, G = radio galaxy, H = HPRQ, high polarized radio quasar, L = LPRQ, low polarized radio quasars, Q = Quasar with no polarization information), Col. (5) is the redshift, Col. (6) is the B-band extinction taken from NED, Col. (7) is the apparent B magnitude in Johnson's photometric system, Col. (8) is the absolute B-magnitude,

TABLE 4

SUMMARY OF THE SPECTROSCOPIC DATA

Sample	Spectral Type	Spectral Region		
		Hβ	Mg II	C IV
(1)	(2)	(3)	(4)	(5)
MOJAVE/2cm	BL	6	···	···
	RG	12	2	1
	HPRQ	8	19	9
	LPRQ	7	18	6
	Q	8	39	19
	Total	41	78	35
MOJAVE-1	BL	4	···	···
	RG	7	1	···
	HPRQ	7	16	9
	LPRQ	6	14	6
	Q	4	15	8
	Total	28	46	23

Col. (9) is the MOJAVE monitoring identification (M1, M2 or 2cm; see Table 1), and Col. (10) is the type of the radio spectra between 0.6 GHz and 22 GHz: $\alpha \gtrsim 0.7$ F = flat, $\alpha < 0.7$ S = steep, C = compact steep spectra, G1 = gigahertz-peaked spectrum with one-sided VLBI jets, G2 = gigahertz-peaked spectrum with two-sided VLBI jets.

7.2. *Spectral Atlas for MOJAVE/2cm AGN Sample*

The Spectral Atlas is presented in Appendix B, it shows 142 spectra corresponding to 123 AGN of the MOJAVE/2cm sample in the observed frame with the redshift information for each source (see Figure 8). The spectra are ordered by right ascension. If multiple spectra are available for a single source they are presented from blue to red wavelengths.

We present the continuum emission and/or line parameters for 41 sources in the Hβ region, 78 in the Mg II region, and 35 in the C IV region. Also, there are 14 sources with information available for both Hβ and Mg II regions, 12 with Mg II, and C IV, and 5 with Hβ, Mg II and C IV. The information for the MOJAVE-1 sample that are included in the Atlas are as follows: 28 sources in the Hβ region, 46 in the Mg II region, and 23 in the C IV region. Table 4 summarizes the data presented for each AGN type. Col. (1) is the sample for which we present the spectroscopic data, Col. (2) is the AGN type, Col. (3)–(5) show the different spectral regions of the continuum emission and/or line parameters for which we report data.

7.3. *Tabular data*

The results of measurements for each parameter of the emission lines and continuum emission for different regions are presented in the Tables 7 to 11 of the Appendix C. The format of these tables is explained in what follows.

Table 7 presents the emission line parameters of the region around Hβ for 41 AGN. Col. (1) is the source name, Col. (2) is the spectrum reference, Col. (3)–(6) are the parameters of the Hβ broad component: FWHM, EW, total flux, and luminosity, respectively, Col. (7)–(10) are the parameters of the [O III] λ5007 line: FWHM, EW, flux and luminosity, respectively. Nine of 41 AGN have only narrow emission lines with FWHM H$\beta \lesssim 1000$ km s^{-1}: 0238−084, 0316+413, 0710+439, 0745+241, 0831+557, 1155+251, 1345+125, 1642+690, and 1957+405.

Table 8 presents the parameters obtained for the emission continuum 5100 Å and the Fe II λ4570: Col. (1) is the source same, Col. (2)–(3) are the flux density and luminosity at 5100 Å, respectively, Col. (4) is the spectral index of the local continuum, Col. (5)–(7) are the total flux, luminosity, and EW of the Fe II λ4570, respectively.

Table 9 presents the continuum emission at 3000 Å, and parameters of the Mg II λ2798 emission line for 78 AGN: Col. (1) is the source name, Col. (2) is the spectrum reference, Col. (3)–(6) are the parameters of the Mg II broad component: FWHM, EW, total flux, and luminosity, respectively, Col. (7)–(8) are the flux density and luminosity at 3000 Å , respectively, and Col. (9) is the spectral index of the local continuum at 3000 Å.

The emission line parameters of the Fe II λ2490 are presented in Table 10: Col. (1) is the source name, Col. (2)–(4) are the total flux, luminosity, and EW, respectively, and Col. (5) is the comment to Fe II λ2490 measurements.

The continuum emission at 1350 Å and parameters of the C IV λ1549 emission line for 35 AGN are presented in Table 11: Col. (1) is the source name, Col. (2) is the spectrum reference, Col. (3)–(6) are the parameters of the C IV broad component: FWHM, EW, total flux, and luminosity, respectively, Col. (7)–(8) are the flux density and luminosity at 1350 Å, and Col. (9) is the spectral index of the local continuum at 1350 Å.

7.4. *Descriptive statistics for different spectral regions*

We have measured the emission line parameters: FWHM, EW, flux, and luminosity, and we obtained the continuum emission flux density and luminosity using our Spectral Atlas of 123 AGN from the MOJAVE/2cm sample. In Table 5 we present the descriptive statistics for each spectral parameter. Columns are as follows: Col. (1) is the parameter, Col. (2) is the spectral type, Col. (3) is the number of sources, Col. (4) is the average value of the parameter, Col.(5) is the standard deviation of the data, and Col. (6) and (7) are the minimum and maximum values of the parameter, respectively. The numbers in parentheses refer to descriptive statistics for the flux-limited sample MOJAVE-1 (M1).

The statistical parameters of the Hβ region are presented for both radio galaxies and quasars because the data for each spectral type are scarce (4 Galaxies, 7 HPRQ, 7 LPRQ, and 6 Q). Note that the radio galaxy 3C 390.3 was excluded from the analysis because of large FWHM Hβ (BC) $\sim 12,000\,\mathrm{km\,s^{-1}}$, as well the BL Lacs and the narrow line objects. The C IV region (9 HPRQ, 6 LPRQ, and 19 Q) was treated similarly. For the Mg II region the statistical analysis was performed for different types of quasars (19 HPRQ, 18 LPRQ, and 39 Q). In this case, two radio galaxies were excluded: 0007+106 and 3C 390.3.

The broad component of the emission line C IV has a larger FWHM C IV (BC) $= 6498 \pm 1515$ km s^{-1} value, between Hβ and Mg II. A caveat here is that the data of each emission line corresponds to a different AGN, and only few sources have data for more than one emission line, as was mentioned in § 7.2.

The continuum luminosity at $\lambda\,L_{1350}$ is larger by a factor of ~ 5 and ~ 30 than the continuum luminosities $\lambda\,L_{3000}$ and $\lambda\,L_{5100}$, respectively.

The FWHM of Mg II is quite similar for different types of quasars (HPRQ, LPRQ, and Q). This parameter has an average value of FWHM Mg II (BC) $= 5108 \pm 946\,\mathrm{km\,s^{-1}}$. In contrast, the EW of Mg II (BC) $= 42 \pm 29$ Å shows a small difference between types. This parameter for quasars with no polarimetry information (Q) is smaller by 36% and 25% than those for HPRQ and LPRQ. The *KS*-test shows that the EW of the Mg II distributions of the HPRQ and LPRQ are different at a confidence level of 95.1% ($P_{KS} = 0.049$), also the distributions of the HPRQ and Q are different at a confidence level of 97.8% ($P_{KS} = 0.011$).

Finally, the *KS*-test between the EW Fe II λ2490 distributions of the HPRQ and LPRQ showed no significant difference ($P_{KS} = 0.314$).

Further analysis related to the emission lines parameters and the properties of the pc-scale jets will be presented in a forthcoming paper.

TABLE 5: Mean values of parameters for continuum and line emission

Parameter (1)	Type (2)	Number (3)	Average (4)	σ (5)	Min. (6)	Max. (7)
FWHM Hβ (BC) [km s^{-1}]	All	24	4055	1331	1670	8600
		(20)	(3957)	(856)	(2650)	(5750)
EW Hβ (BC) [Å]	All	24	56	24	13	125
		(20)	(57)	(26)	(13)	(125)
$L_{\mathrm{H}\beta\,(\mathrm{BC})}$ [10^{42} erg s^{-1}]	All	24	40	50	1	182
		(20)	(37)	(44)	(1)	(182)
EW Fe II λ4570 [Å]	All	22	18	17	2	69
		(17)	(19)	(17)	(2)	(69)
L_{4570} [10^{41} erg s^{-1}]	All	22	96	96	2	342
		(17)	(98)	(99)	(2)	(342)
FWHM [O III] λ5007 [km s^{-1}]	All	35	767	382	360	1716
		(24)	(731)	(328)	(360)	(1394)
EW [O III] λ5007 [Å]	All	35	39	62	0.2	380
		(24)	(43)	(75)	(5)	(380)
$L_{[\mathrm{O\,III}]}$ [10^{42} erg s^{-1}]	All	35	14	33	0.004	191
		(24)	(10)	(13)	(0.004)	(50)
λL_{5100} [10^{44} erg s^{-1}]	All	41	31	42	0.01	181
		(28)	(34)	(43)	(0.006)	(181)
FWHM Mg II (BC) [km s^{-1}]	All	76	5108	946	2445	8752
		(45)	(5174)	(663)	(3735)	(7495)
	HPRQ	19	5118	960	2565	7495
		(16)	(5272)	(789)	(4245)	(7495)
	LPRQ	18	5151	1063	3735	8752
		(14)	(4991)	(599)	(3735)	(5583)
	Q	39	5083	908	2445	6849
		(15)	(5239)	(578)	(4287)	(6266)
EW Mg II (BC) [Å]	All	76	36	24	6	177
		(45)	(33)	(27)	(6)	(177)
	HPRQ	19	27	18	6	74
		(16)	(29)	(19)	(6)	(74)
	LPRQ	18	31	12	15	53
		(14)	(30)	(11)	(15)	(53)
	Q	39	42	29	11	177
		(15)	(40)	(41)	(13)	(177)
$L_{\mathrm{Mg\,II(BC)}}$ [10^{42} erg s^{-1}]	All	76	177	695	7	6091
		(45)	(229)	(899)	(11)	(6091)
	HPRQ	19	53	34	7	126
		(16)	(50)	(30)	(11)	(126)
	LPRQ	18	476	1407	35	6091
		(14)	(587)	(1591)	(47)	(6091)
	Q	39	99	97	12	438
		(15)	(85)	(60)	(17)	(196)
EW Fe II λ2490 [Å]	All	67	54	26	6	128
		(40)	(50)	(26)	(6)	(128)
	HPRQ	18	41	21	6	79
		(15)	(39)	(22)	(6)	(79)
	LPRQ	16	47	17	18	74
		(12)	(47)	(17)	(18)	(67)
	Q	33	65	27	21	128
		(13)	(64)	(33)	(22)	(128)
L_{2490} [10^{42} erg s^{-1}]	All	67	1614	10,772	31	88,402
		(40)	(2456)	(13,941)	(40)	(88,402)
	HPRQ	18	137	101	40	451
		(15)	(118)	(68)	(40)	(275)

	LPRQ	16	5863	22014	36	88402
		(12)	(7760)	(25,400)	(100)	(88,402)
	Q	33	359	535	31	2760
		(13)	(257)	(153)	(46)	(521)
λL_{3000} [10^{44} erg s^{-1}]	All	76	204	936	8	8205
		(45)	(287)	(1212)	(8)	(8205)
	HPRQ	19	88	70	13	237
		(16)	(84)	(70)	(13)	(237)
	LPRQ	18	592	1905	23	8205
		(14)	(735)	(2155)	(33)	(8205)
	Q	39	82	90	8	386
		(15)	(84)	(73)	(8)	(223)
FWHM C IV (BC) [km s^{-1}]	All	34	6498	1515	2818	9150
		(23)	(6640)	(1500)	(3445)	(9150)
EW C IV (BC) [Å]	All	34	29	17	10	87
		(23)	(29)	(17)	(10)	(87)
$L_{\rm C\,IV\,(BC)}$[10^{42} erg s^{-1}]	All	34	817	2063	20	11,345
		(23)	(857)	(2314)	(27)	(11,345)
λL_{1350} [10^{44} erg s^{-1}]	All	34	983	3363	5	19,566
		(23)	(1199)	(4043)	(24)	(19,566)

8. SUMMARY

For the first time an optical spectroscopic atlas with intermediate resolution data of the bright part of the MOJAVE/2cm sample, comprised by core-dominated AGN at 15 GHz, is presented.

The parameters obtained from the spectra of 123 sources, such as FWHM, EW, fluxes, and luminosities of various emission lines (Hβ, [O III] λ5007, Mg II λ2798, and/or C IV λ1549), and their corresponding continuum emission are presented together with the descriptive statistics of these parameters. The luminosities and equivalent widths of the Fe II λ4570 and Fe II λ2490 are presented for 22 and 67 sources, respectively.

We also carried out a photometric calibration that allowed us to present a homogeneous B–band photometric data for 242 AGN of the MOJAVE/2cm sample. Using these data, Arshakian et al. (2011, 2010b) have discussed the relations between optical, radio, and γ-ray emission of 135 AGN from the flux-density-limited MOJAVE-1 sample. Torrealba et al. (2011) used the photometric data of 233 AGN of the MOJAVE/2cm sample to confirm the relations between the optical and 15 GHz emission found for MOJAVE-1. In a forthcoming paper, we will present the results of analysis of the emission line parameters and the properties of the pc-scale jets. Preliminary results about this study have been published in Arshakian et al. (2005), Torrealba et al. (2008), Torrealba (2010), and Hovatta et al. (2010).

The authors want to acknowledge an anonymous referee for very useful comments and suggestions, which helped to improve this work. We also are grateful to Dr. C. R. Lawrence for kindly providing us his spectroscopic data. We thank Marianne Vestergaard for kindly providing us the Fe II template which was used in this work. Special thanks are given to the technical staff

and night assistant of the OAN–SPM and OAGH. This work is supported by CONACyT basic research grants 48484-F, 54480, 151494 (México).

This research has made use of (1) data that were acquired at Observatorio Astronómico Nacional in San Pedro Mártir (OAN–SPM), México and at Observatorio Astronómico Guillermo Haro, in Cananea, Sonora (OAGH); (3) the USNO-B catalog (Monet et al. 2003); (4) the MAPS Catalog of POSS I supported by the University of Minnesota (the APS databases can be accessed at http://aps.umn.edu/); (5) the NASA/IPAC Extragalactic Database (NED) which is operated by the Jet Propulsion Laboratory, California Institute of Technology, under contract with the National Aeronautics and Space Administration; (6) The *SDSS*. Funding for the *SDSS*[13] and *SDSS-II* has been provided by the Alfred P. Sloan Foundation, the Participating Institutions, the National Science Foundation, the U.S. Department of Energy, the National Aeronautics and Space Administration, the Japanese Monbukagakusho, the Max Planck Society, and the Higher Education Funding Council for England. The *SDSS* is managed by the Astrophysical Research Consortium for the Participating Institutions. The Participating Institutions are the American Museum of Natural History, Astrophysical Institute Potsdam, University of Basel, University of Cambridge, Case Western Reserve University, University of Chicago, Drexel University, Fermilab, the Institute for Advanced Study, the Japan Participation Group, Johns Hopkins University, the Joint Institute for Nuclear Astrophysics, the Kavli Institute for Particle Astrophysics and Cosmology, the Korean Scientist Group, the Chinese Academy of Sciences (LAMOST), Los Alamos National Laboratory, the Max-Planck-Institute for Astronomy (MPIA), the Max-Planck-Institute for Astrophysics (MPA), New Mexico State University, Ohio State University, University of Pittsburgh, University of Portsmouth, Princeton University, the United States Naval Observatory, and the University of Washington. (7) The Multimission Archive at the Space Telescope Science Institute (MAST). STScI is operated by the Association of Universities for Research in Astronomy, Inc., under NASA contract NAS5-26555. Support for MAST for non-HST data is provided by the NASA Office of Space Science via grant NNX09AF08G and by other grants and contracts.

[13]The *SDSS* Web Site is http://www.sdss.org/.

APPENDICES

A. MOJAVE/2CM AGN SAMPLE

TABLE 6

MOJAVE/2CM AGN SAMPLE

IAU Name	R.A. (2000)	Dec. (2000)	Optical Class	z	A_B	B_J	M_B	MOJAVE Id.	Radio Spectra
0003−066	00 06 13.89	−06 23 35.33	B	0.347	0.157	20.12	−20.74	M1	F
0007+106	00 10 31.03	+10 58 29.70	G	0.089	0.422	13.54	−24.37	M1	F
0014+813	00 17 8.475	+81 35 08.14	Q	3.387	0.810	17.22	−28.44	2cm	F
0016+731	00 19 45.78	+73 27 30.02	L	1.781	1.376	18.88	−25.46	M1	F
0026+346	00 29 14.24	+34 56 32.26	G	0.517	0.466	20.99	−20.73	2cm	F
0035+413	00 38 24.84	+41 37 06.00	Q	1.353	0.268	21.34	−22.43	2cm	F
0039+230	00 42 4.54	+23 20 01.06	U	···	0.124	20.08	···	2cm	F
0048−097	00 50 41.33	−09 29 05.20	B	···	0.139	16.79	···	M1	F
0055+300	00 57 48.93	+30 21 08.20	G	0.017	0.279	13.05	−21.26	M2	F
0059+581	01 02 45.76	+58 24 11.11	Q	0.644	2.374	19.24	−22.94	M1	F
0106+013	01 08 38.77	+01 35 00.32	H	2.099	0.105	18.75	−25.94	M1	F
0108+388	01 11 37.39	+39 06 28.10	G	0.668	0.204	16.17	−26.10	M2	G2
0109+224	01 12 05.82	+22 44 38.79	B	0.265	0.161	15.60	−24.67	M1	F
0112−017	01 15 17.10	−01 27 04.58	Q	1.365	0.267	17.47	−26.32	2cm	F
0113−118	01 16 12.52	−11 36 15.43	Q	0.672	0.125	18.09	−24.19	M2	F
0119+041	01 21 56.86	+04 22 24.73	H	0.637	0.152	18.64	−23.52	2cm	F
0119+115	01 21 41.67	+11 49 50.60	Q	0.570	0.138	19.64	−22.29	M1	F
0122−003	01 25 28.84	−00 05 55.96	Q	1.077	0.138	16.41	−26.88	M2	F
0133+476	01 36 58.59	+47 51 29.10	H	0.859	0.658	17.43	−25.37	M1	F
0133−203	01 35 37.51	−20 08 45.89	Q	1.141	0.075	18.31	−25.10	2cm	F
0138−097	01 41 25.83	−09 28 43.67	B	0.733	0.127	17.68	−24.79	2cm	F
0146+056	01 49 22.37	+05 55 53.57	Q	2.345	0.265	20.32	−24.59	2cm	F
0149+218	01 52 18.06	+22 07 07.70	Q	1.320	0.324	19.37	−24.35	M2	F
0153+744	01 57 34.88	+74 42 43.00	Q	2.341	2.090	17.98	−26.93	2cm	F
0201+113	02 03 46.72	+11 34 45.60	Q	3.610	0.617	21.85	−23.94	2cm	F
0202+149	02 04 50.41	+15 14 11.04	H	0.405	0.230	22.40	−18.79	M1	F
0202+319	02 05 04.92	+32 12 30.10	L	1.466	0.254	16.54	−27.40	M1	F
0212+735	02 17 30.81	+73 49 32.62	H	2.367	3.212	20.30	−24.63	M1	F
0215+015	02 17 48.95	+01 44 49.60	H	1.715	0.144	20.17	−24.09	M1	F
0218+357	02 21 05.47	+35 56 13.72	Q	0.944	0.293	20.28	−22.73	2cm	F
0221+067	02 24 28.49	+06 59 23.50	Q	0.511	0.321	20.65	−21.04	2cm	F
0224+671	02 28 50.05	+67 21 03.00	Q	0.523	4.443	20.91	−20.83	M1	F
0234+285	02 37 52.40	+28 48 08.99	H	1.207	0.677	19.08	−24.45	M1	F
0235+164	02 38 38.93	+16 36 59.28	B	0.940	0.341	20.21	−22.79	M1	F
0238−084	02 41 04.71	−08 15 21.50	G	0.005	0.114	12.90	−18.76	M1	F
0248+430	02 51 34.54	+43 15 15.83	Q	1.310	0.463	14.77	−28.93	2cm	F
0300+470	03 03 35.24	+47 16 16.20	B	···	1.132	18.21	···	M1	F
0310+013	03 12 43.60	+01 33 17.54	Q	0.664	0.658	18.39	−23.86	2cm	F
0316+162	03 18 57.76	+16 28 32.34	Q	0.907	0.673	23.31	···	2cm	G1
0316+413	03 19 48.16	+41 30 42.10	G	0.018	0.703	12.85	−21.59	M1	F
0333+321	03 36 30.49	+32 18 28.70	L	1.259	3.244	18.18	−25.44	M1	F
0336−019	03 39 30.93	−01 46 35.80	H	0.852	0.377	17.31	−25.48	M1	F
0355+508	03 59 29.74	+50 57 50.16	Q	1.510	6.362	···	···	M2	F
0402−362	04 03 53.75	−36 05 01.91	Q	1.417	0.022	16.81	−27.05	2cm	G
0403−132	04 05 34.00	−13 08 13.60	H	0.571	0.250	17.71	−24.22	M1	F
0405−385	04 06 59.07	−38 26 27.80	Q	1.285	0.024	19.18	−24.48	2cm	F

TABLE 6 (CONTINUED)

IAU Name	R.A. (2000)	Dec. (2000)	Optical Class	z	A_B	B_J	M_B	MOJAVE Id.	Radio Spectra
0415+379	04 18 21.27	+38 01 35.51	G	0.049	7.107	20.36	−16.25	M1	S
0420+022	04 22 52.22	+02 19 26.94	Q	2.277	0.936	20.41	−24.44	2cm	F
0420−014	04 23 15.80	−01 20 33.06	H	0.914	0.567	17.65	−25.29	M1	F
0422+004	04 24 46.84	00 36 06.30	B	···	0.436	16.56	···	M1	F
0429+415	04 32 36.50	+41 38 28.43	Q	1.022	2.413	19.13	−24.04	M2	C
0430+052	04 33 11.08	+05 21 15.90	G	0.033	1.283	16.01	−19.74	M1	F
0438−436	04 40 17.18	−43 33 08.60	Q	2.852	0.060	19.58	−25.73	2cm	F
0440−003	04 42 38.66	+00 17 43.47	Q	0.844	0.227	19.47	−23.30	M2	F
0446+112	04 49 07.67	+11 21 28.50	U	···	2.170	21.00	···	M1	F
0454+844	05 08 42.52	+84 32 04.50	B	0.112	0.412	18.61	−19.80	M2	F
0454−234	04 57 03.18	−23 24 52.02	Q	1.003	0.204	18.58	−24.55	M2	F
0458−020	05 01 12.81	−01 59 14.26	H	2.286	0.327	19.05	−25.82	M1	F
0521−365	05 22 57.99	−36 27 31.00	G	0.055	0.169	12.35	−24.51	2cm	S
0524+034	05 27 32.70	+03 31 31.45	B	···	0.681	18.99	···	2cm	F
0528+134	05 30 56.41	+13 31 55.18	H	2.070	3.621	20.37	−24.29	M1	F
0529+075	05 32 38.99	+07 32 43.30	Q	1.254	1.352	19.75	−23.86	M1	F
0529+483	05 33 15.86	+48 22 52.80	Q	1.162	1.767	20.62	−22.83	M1	F
0537−286	05 39 54.28	−28 39 55.95	Q	3.104	0.106	20.00	−25.49	2cm	F
0552+398	05 55 30.80	+39 48 49.16	Q	2.363	1.862	18.09	−26.84	M1	F
0602+673	06 07 52.67	+67 20 55.42	Q	1.970	0.676	21.05	−23.50	2cm	F
0605−085	06 07 59.69	−08 34 49.98	Q	0.872	2.572	18.77	−24.07	M1	F
0607−157	06 09 40.93	−15 42 40.70	Q	0.324	1.107	18.77	−21.94	M1	F
0615+820	06 26 03.04	+82 02 25.50	Q	0.710	0.357	18.39	−24.01	2cm	F
0642+449	06 46 32.02	+44 51 16.59	Q	3.396	0.483	19.63	−26.05	M1	F
0648−165	06 50 24.58	−16 37 39.70	U	···	2.456	···	···	M1	F
0707+476	07 10 46.10	+47 32 11.14	Q	1.292	0.342	14.33	−29.34	M2	F
0710+439	07 13 38.17	+43 49 17.00	G	0.518	0.309	19.98	−21.74	M2	G2
0711+356	07 14 24.82	+35 34 39.80	Q	1.620	0.246	17.85	−26.30	2cm	G
0716+714	07 21 53.46	+71 20 36.20	B	···	0.132	14.69	···	M1	F
0723−008	07 25 50.64	−00 54 56.30	B	0.127	0.324	17.66	−21.02	M2	F
0727−115	07 30 19.11	−11 41 12.60	Q	1.591	1.271	···	···	M1	F
0730+504	07 33 52.52	+50 22 09.00	Q	0.720	0.273	19.47	−22.96	M1	F
0735+178	07 38 07.42	+17 42 19.20	B	···	0.151	16.47	···	M1	F
0736+017	07 39 18.09	+01 37 03.17	H	0.191	0.549	17.25	−22.31	M1	F
0738+313	07 41 10.73	+31 11 59.10	Q	0.631	0.202	16.25	−25.89	M1	F
0742+103	07 45 33.06	+10 11 12.69	Q	2.624	0.111	···	···	M1	G1
0745+241	07 48 36.11	+24 00 24.15	H	0.409	0.244	19.41	−21.80	M2	F
0748+126	07 50 52.04	+12 31 04.83	Q	0.889	0.133	17.49	−25.39	M1	F
0754+100	07 57 06.67	+09 56 34.00	B	0.266	0.097	15.29	−24.99	M1	F
0804+499	08 08 39.66	+49 50 36.50	H	1.436	0.228	14.90	−28.99	M1	F
0805−077	08 08 15.53	−07 51 09.80	Q	1.837	0.613	17.96	−26.45	M1	F
0808+019	08 11 26.71	+01 46 52.30	B	1.148	0.142	18.03	−25.39	M1	F
0814+425	08 18 16.00	+42 22 45.41	B	0.245	0.274	20.05	−20.05	M1	F
0821+394	08 24 55.48	+39 16 41.90	Q	1.216	0.197	18.19	−25.35	2cm	F
0823+033	08 25 50.33	+03 09 24.52	B	0.506	0.197	15.53	−26.14	M1	F
0827+243	08 30 52.08	+24 10 59.80	L	0.940	0.142	17.01	−25.99	M1	F
0829+046	08 31 48.89	+04 29 38.70	B	0.174	0.141	14.64	−24.80	M1	F
0831+557	08 34 54.90	+55 34 21.07	U	0.240	0.189	19.51	−20.55	2cm	F
0834−201	08 36 39.26	−20 16 59.70	Q	2.752	0.432	19.36	−25.88	M2	F
0836+710	08 41 24.37	+70 53 42.10	L	2.218	0.132	16.78	−28.02	M1	F
0838+133	08 40 47.68	+13 12 23.88	Q	0.681	0.403	17.89	−24.43	M1	F
0850+581	08 54 41.99	+57 57 29.95	L	1.322	0.232	18.24	−25.48	M2	F
0851+202	08 54 48.88	+20 06 30.70	B	0.306	0.122	14.53	−26.05	M1	F

TABLE 6 (CONTINUED)

IAU Name	R.A. (2000)	Dec. (2000)	Optical Class	z	A_B	B_J	M_B	MOJAVE Id.	Radio Spectra
0859+470	09 03 04.05	+46 51 04.10	L	1.462	0.085	18.61	−25.32	2cm	F
0859−140	09 02 16.83	−14 15 30.80	Q	1.339	0.269	16.46	−27.29	M2	C
0906+015	09 09 10.09	+01 21 35.80	H	1.024	0.148	16.76	−26.41	M1	F
0917+449	09 20 58.45	+44 41 53.98	Q	2.180	0.089	18.82	−25.94	M2	F
0917+624	09 21 36.23	+62 15 52.10	Q	1.446	0.203	19.63	−24.28	M1	F
0919−260	09 21 29.35	−26 18 43.38	Q	2.300	0.574	18.90	−25.97	2cm	G
0923+392	09 27 03.01	+39 02 20.85	L	0.695	0.062	16.61	−25.75	M1	F
0945+408	09 48 55.33	+40 39 44.60	L	1.249	0.060	17.62	−25.98	M1	F
0953+254	09 56 49.89	+25 15 16.00	L	0.712	0.158	16.73	−25.67	M2	F
0954+658	09 58 47.24	+65 33 54.82	B	0.367	0.495	16.62	−24.36	M2	F
0955+476	09 58 19.67	+47 25 07.80	Q	1.882	0.064	18.31	−26.14	M1	F
1012+232	10 14 47.09	+23 01 16.80	Q	0.565	0.106	17.50	−24.41	2cm	F
1015+359	10 18 10.98	+35 42 39.44	Q	1.226	0.050	17.94	−25.62	M2	F
1032−199	10 35 02.21	−20 11 34.70	Q	2.198	0.192	18.00	−26.78	2cm	F
1034−293	10 37 16.08	−29 34 02.81	Q	0.312	0.221	17.52	−23.11	M2	F
1036+054	10 38 46.77	+05 12 29.00	Q	0.473	0.110	20.20	−21.32	M1	F
1038+064	10 41 17.16	+06 10 16.90	Q	1.265	0.107	16.46	−27.17	M1	F
1045−188	10 48 06.62	−19 09 35.70	Q	0.595	0.164	17.77	−24.25	M1	F
1049+215	10 51 48.79	+21 19 52.35	Q	1.300	0.109	18.23	−25.45	2cm	F
1055+018	10 58 29.60	+01 33 58.82	H	0.890	0.116	17.90	−24.98	M1	F
1055+201	10 58 17.90	+19 51 51.40	Q	1.110	0.106	18.51	−24.84	2cm	F
1101+384	11 04 27.34	+38 12 31.50	B	0.031	0.066	13.61	−22.01	M2	F
1116+128	11 18 57.30	+12 34 41.72	Q	2.118	0.109	18.40	−26.30	2cm	F
1124−186	11 27 04.46	−18 57 17.80	H	1.048	0.187	19.43	−23.80	M1	F
1127−145	11 30 07.05	−14 49 27.00	Q	1.184	0.158	16.75	−26.74	M1	F
1128+385	11 30 53.28	+38 15 18.55	Q	1.733	0.109	19.12	−25.17	M2	F
1144+402	11 46 58.30	+39 58 34.30	Q	1.089	0.075	18.61	−24.70	2cm	F
1145−071	11 47 51.62	−07 24 41.40	Q	1.342	0.180	18.43	−25.32	2cm	F
1148−001	11 50 43.86	−00 23 54.38	Q	1.980	0.098	16.84	−27.72	M2	F
1150+812	11 53 12.49	+80 58 29.10	Q	1.250	0.332	19.73	−23.87	M1	F
1155+251	11 58 25.82	+24 50 18.00	Q	0.202	0.086	19.66	−20.03	2cm	F
1156+295	11 59 31.83	+29 14 44.00	H	0.729	0.084	16.94	−25.51	M1	F
1213−172	12 15 46.75	−17 31 45.40	U	···	0.253	···	···	M1	F
1219+044	12 22 22.50	+04 13 16.00	H	0.965	0.085	17.27	−25.78	M1	F
1219+285	12 21 31.70	+28 13 58.40	B	0.102	0.097	17.09	−21.11	M2	F
1222+216	12 24 54.45	+21 22 46.30	Q	0.432	0.101	17.77	−23.57	M1	F
1226+023	12 29 06.70	+02 03 08.60	L	0.158	0.089	16.52	−22.66	M1	F
1228+126	12 30 49.42	+12 23 28.00	G	0.004	0.096	11.12	−20.05	M1	S
1244−255	12 46 46.80	−25 47 49.29	H	0.633	0.375	17.31	−24.86	M2	F
1253−055	12 56 11.16	−05 47 21.52	H	0.536	0.123	16.02	−25.78	M1	F
1255−316	12 57 59.06	−31 55 16.85	Q	1.924	0.380	18.64	−25.86	2cm	F
1302−102	13 05 33.01	−10 33 19.30	L	0.278	0.184	15.20	−25.18	M2	F
1308+326	13 10 28.66	+32 20 43.78	H	0.997	0.060	19.83	−23.29	M1	F
1313−333	13 16 07.99	−33 38 59.17	Q	1.210	0.265	18.22	−25.31	2cm	F
1323+321	13 26 16.51	+31 54 09.52	G	0.370	0.065	21.21	−19.78	2cm	G2
1324+224	13 27 00.86	+22 10 50.10	Q	1.400	0.072	17.95	−25.89	M1	F
1328+307	13 31 08.31	+30 30 32.90	Q	0.846	0.050	17.12	−25.65	2cm	C
1334−127	13 37 39.80	−12 57 24.70	H	0.539	0.323	18.73	−23.08	M1	F
1345+125	13 47 33.49	+12 17 23.50	G	0.121	0.145	17.33	−21.24	M2	G2
1354+195	13 57 04.45	+19 19 07.30	Q	0.719	0.260	16.03	−26.39	2cm	F
1354−152	13 57 11.33	−15 27 29.00	Q	1.890	0.406	17.53	−26.94	2cm	F
1402+044	14 05 01.12	+4 15 35.82	Q	3.211	0.115	20.62	−24.94	2cm	F
1404+286	14 07 00.39	+28 27 14.00	G	0.077	0.079	16.84	−20.75	M2	G2

TABLE 6 (CONTINUED)

IAU Name	R.A. (2000)	Dec. (2000)	Optical Class	z	A_B	B_J	M_B	MOJAVE Id.	Radio Spectra
1413+135	14 15 58.81	+13 20 23.71	B	0.247	0.106	21.41	−18.71	M1	F
1417+385	14 19 46.61	+38 21 48.40	Q	1.831	0.036	20.35	−24.05	M1	F
1418+546	14 19 46.60	+54 23 14.79	B	0.152	0.058	14.79	−24.28	M2	F
1424+366	14 26 37.08	+36 25 09.59	Q	1.091	0.035	18.89	−24.42	2cm	F
1458+718	14 59 07.61	+71 40 19.90	L	0.904	0.110	16.95	−25.96	M1	C
1502+106	15 04 25.02	+10 29 39.20	H	1.839	0.138	19.60	−24.81	M1	F
1504+377	15 06 09.61	+37 30 51.20	Q	0.674	0.055	21.49	−20.80	2cm	F
1504−166	15 07 04.88	−16 52 30.50	H	0.876	0.410	20.19	−22.66	M1	F
1508−055	15 10 53.59	−05 43 07.10	Q	1.191	0.367	17.18	−26.32	M2	C
1510−089	15 12 50.53	−09 05 59.70	H	0.360	0.416	16.10	−24.84	M1	F
1511−100	15 13 44.98	+10 12 00.40	Q	1.513	0.456	18.77	−25.23	2cm	F
1514+004	15 16 40.22	+00 15 01.91	G	0.052	0.238	17.05	−19.69	M2	F
1514−241	15 17 41.80	−24 22 19.60	B	0.049	0.595	16.91	−19.70	M2	F
1519−273	15 22 37.77	−27 30 11.00	B	1.297	1.026	18.12	−25.56	2cm	F
1532+016	15 34 52.45	+01 31 04.21	Q	1.420	0.218	19.67	−24.20	M2	F
1538+149	15 40 49.51	+14 47 46.00	B	0.605	0.238	15.91	−26.14	M1	F
1546+027	15 49 29.43	+02 37 01.16	H	0.414	0.495	17.95	−23.28	M1	F
1548+056	15 50 35.27	+05 27 10.47	H	1.422	0.289	18.16	−25.71	M1	F
1555+001	15 57 51.52	−00 01 50.50	Q	1.772	0.602	19.55	−24.78	2cm	F
1606+106	16 08 46.20	+10 29 07.78	Q	1.226	0.270	18.10	−25.46	M1	F
1607+268	16 09 13.32	+26 41 29.04	G	0.473	0.228	···	···	M2	G1
1611+343	16 13 41.07	+34 12 48.10	L	1.397	0.077	17.67	−26.17	M1	F
1622−253	16 25 46.89	−25 27 38.30	Q	0.786	4.960	20.89	−21.72	M2	F
1622−297	16 26 06.02	−29 51 26.97	Q	0.815	1.861	18.06	−24.63	M2	F
1624+416	16 25 57.67	+41 34 40.63	Q	2.550	0.035	20.00	−25.09	2cm	F
1633+382	16 35 15.49	+38 08 04.50	H	1.814	0.048	18.19	−26.18	M1	F
1637+574	16 38 13.45	+57 20 23.90	L	0.751	0.054	16.68	−25.84	M1	F
1638+398	16 40 29.63	+39 46 46.03	Q	1.666	0.044	18.49	−25.71	M1	F
1641+399	16 42 58.81	+39 48 36.90	H	0.593	0.057	15.99	−26.02	M1	F
1642+690	16 42 07.84	+68 56 39.76	H	0.751	0.165	20.02	−22.50	M2	F
1652+398	16 53 52.26	+39 45 36.70	B	0.033	0.084	15.15	−20.60	M2	F
1655+077	16 58 09.01	+07 41 27.54	H	0.621	0.661	20.13	−21.98	M1	F
1656+053	16 58 33.48	+05 15 16.40	H	0.879	0.684	16.84	−26.01	2cm	F
1656+477	16 58 02.77	+47 37 49.24	Q	1.622	0.091	17.15	−27.00	2cm	F
1726+455	17 27 27.65	+45 30 39.70	Q	0.717	0.105	18.79	−23.62	M1	F
1730−130	17 33 02.70	−13 04 49.55	H	0.902	2.203	21.56	−21.35	M1	F
1739+522	17 40 36.07	+52 11 43.50	H	1.379	0.153	18.20	−25.61	M1	F
1741−038	17 43 58.85	−03 50 04.62	H	1.054	2.457	19.76	−23.49	M1	F
1749+096	17 51 32.82	+09 39 00.60	B	0.322	0.779	18.48	−22.20	M1	F
1749+701	17 48 32.90	+70 05 50.70	B	0.770	0.133	16.41	−26.16	M2	F
1751+288	17 53 42.47	+28 48 04.90	Q	1.118	0.250	20.77	−22.59	M1	F
1758+388	18 00 24.76	+38 48 30.70	Q	2.092	0.116	17.76	−26.92	M1	F
1800+440	18 01 32.42	+44 04 20.60	Q	0.663	0.264	16.98	−25.27	M1	F
1803+784	18 00 45.70	+78 28 04.20	B	0.680	0.225	15.35	−26.95	M1	F
1807+698	18 06 50.71	+69 49 28.20	B	0.051	0.155	17.00	−19.70	M1	F
1821+107	18 24 02.86	+10 44 23.77	Q	1.364	0.818	18.28	−25.50	2cm	G
1823+568	18 24 07.06	+56 51 01.49	B	0.664	0.264	18.60	−23.65	M1	F
1828+487	18 29 31.78	+48 44 46.20	L	0.692	0.333	17.18	−25.16	M1	C
1845+797	18 42 08.89	+79 46 16.70	G	0.056	0.308	13.76	−23.14	M2	S
1849+670	18 49 16.07	+67 05 41.60	Q	0.657	0.243	16.18	−26.05	M1	F
1901+319	19 02 55.94	+31 59 41.70	Q	0.635	0.523	18.26	−23.90	M2	C
1908−201	19 11 09.65	−20 06 55.11	Q	1.119	0.696	18.33	−25.04	M2	F
1921−293	19 24 51.04	−29 14 30.30	H	0.352	0.536	18.34	−22.55	M2	F

TABLE 6 (CONTINUED)

IAU Name	R.A. (2000)	Dec. (2000)	Optical Class	z	A_B	B_J	M_B	MOJAVE Id.	Radio Spectra
1928+738	19 27 48.45	+73 58 01.80	L	0.302	0.574	15.71	−24.85	M1	F
1936−155	19 39 26.65	−15 25 43.00	H	1.657	0.690	19.37	−24.82	M1	F
1937−101	19 39 57.26	−10 02 41.52	Q	3.787	0.911	18.55	−27.34	2cm	F
1954+513	19 55 42.83	+51 31 48.60	L	1.223	0.650	19.14	−24.41	M2	F
1954−388	19 57 59.82	−38 45 06.36	Q	0.630	0.347	18.83	−23.31	2cm	F
1957+405	19 59 28.34	+40 44 02.02	G	0.056	1.644	13.79	−23.11	M1	S
1958−179	20 00 57.09	−17 48 57.60	H	0.650	0.573	17.86	−24.35	M1	F
2000−330	20 03 24.12	−32 51 45.13	Q	3.783	0.562	19.48	−26.41	2cm	G
2005+403	20 07 44.94	+40 29 48.61	Q	1.736	2.995	19.78	−24.51	M1	F
2007+777	20 05 31.08	+77 52 43.30	B	0.342	0.696	17.07	−23.75	M2	F
2008−159	20 11 15.71	−15 46 40.20	Q	1.180	0.613	17.29	−26.19	M1	F
2010+463	20 12 05.64	+46 28 55.78	B	···	2.953	17.47	···	2cm	F
2021+317	20 23 19.01	+31 53 02.31	U	···	4.565	···	···	M1	F
2021+614	20 22 06.68	+61 36 58.81	G	0.227	0.884	19.83	−20.11	M1	F
2029+121	20 31 54.99	+12 19 41.34	Q	1.215	0.349	···	···	M2	F
2037+511	20 38 37.03	+51 19 12.60	Q	1.686	4.732	19.88	−24.35	M1	F
2059+034	21 01 38.83	+03 41 31.32	Q	1.015	0.447	17.24	−25.92	2cm	F
2113+293	21 15 29.41	+29 33 38.37	Q	1.514	0.564	20.05	−23.95	M2	F
2121+053	21 23 44.61	+05 35 22.30	H	1.941	0.313	17.98	−26.54	M1	F
2126−158	21 29 12.18	−15 38 41.04	Q	3.280	0.344	17.24	−28.36	M2	F
2128+048	21 30 32.97	+05 02 17.70	G	0.990	0.257	23.71	−19.40	2cm	G2
2128−123	21 31 35.35	−12 07 04.50	L	0.501	0.265	15.63	−26.02	M1	F
2131−021	21 34 10.31	−01 53 17.24	B	1.285	0.238	18.74	−24.92	M1	F
2134+004	21 36 38.58	+00 41 54.20	L	1.932	0.281	16.93	−27.58	M1	F
2136+141	21 39 01.31	+14 23 35.99	Q	2.427	0.427	18.74	−26.24	M1	F
2144+092	21 47 10.16	+09 29 46.68	Q	1.113	0.310	18.41	−24.95	M2	F
2145+067	21 48 05.45	+06 57 38.61	L	0.990	0.345	16.50	−26.63	M1	F
2155−152	21 58 06.37	−15 01 09.00	H	0.672	0.207	17.65	−24.63	M1	F
2200+420	22 02 43.29	+42 16 39.98	B	0.069	1.420	15.62	−21.73	M1	F
2201+171	22 03 26.89	+17 25 48.20	Q	1.076	0.240	19.50	−23.78	M1	F
2201+315	22 03 14.97	+31 45 38.27	L	0.295	0.534	14.98	−25.55	M1	F
2209+236	22 12 05.96	+23 55 40.59	Q	1.125	0.330	19.60	−23.78	M1	F
2216−038	22 18 52.03	−03 35 36.80	Q	0.901	0.409	16.87	−26.04	M1	F
2223−052	22 25 47.25	−04 57 01.39	H	1.404	0.325	18.03	−25.82	M1	F
2227−088	22 29 40.17	−08 32 54.10	H	1.560	0.221	17.74	−26.33	M1	F
2230+114	22 32 36.40	+11 43 50.89	H	1.037	0.312	17.08	−26.13	M1	F
2234+282	22 36 22.47	+28 28 57.42	H	0.795	0.273	19.55	−23.09	M2	F
2243−123	22 46 18.23	−12 06 51.28	H	0.632	0.215	16.26	−25.88	M1	F
2251+158	22 53 57.74	+16 08 53.56	H	0.859	0.462	16.51	−26.29	M1	F
2255−282	22 58 06.05	−27 58 20.90	Q	0.927	0.145	16.54	−26.43	M2	F
2318+049	23 20 44.94	+05 13 50.20	Q	0.623	0.282	18.53	−23.59	2cm	F
2329−162	23 31 38.65	−15 56 57.01	Q	1.153	0.111	20.06	−23.37	2cm	F
2331+073	23 34 12.82	+07 36 27.50	Q	0.401	0.353	16.40	−24.77	M1	F
2345−167	23 48 02.60	−16 31 12.02	H	0.576	0.112	18.50	−23.45	M1	F
2351+456	23 54 21.68	+45 53 04.20	Q	1.986	0.527	20.50	−24.07	M1	F

B. SPECTROSCOPIC ATLAS

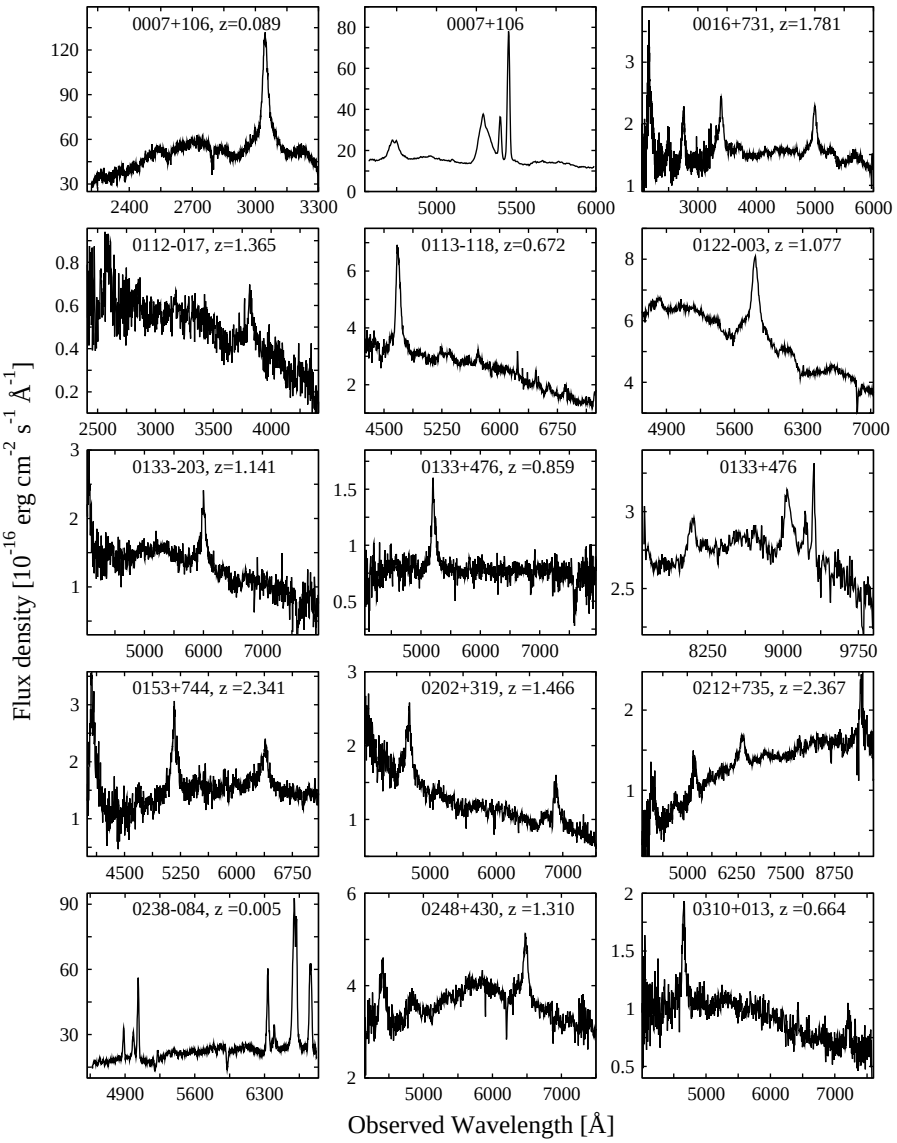

Fig. 8. Spectra for the 123 objects of the MOJAVE/2cm sample that was available to study the Hβ region, and/or Mg II λ2798/C IV λ1549; the abcissa is the observed wavelength in Å and the ordinate is the flux density in units of $10^{-16}\,\mathrm{erg\,cm^{-2}\,s^{-1}\,\AA^{-1}}$, the name and the redshift of the source are shown in the top of the corresponding frame.

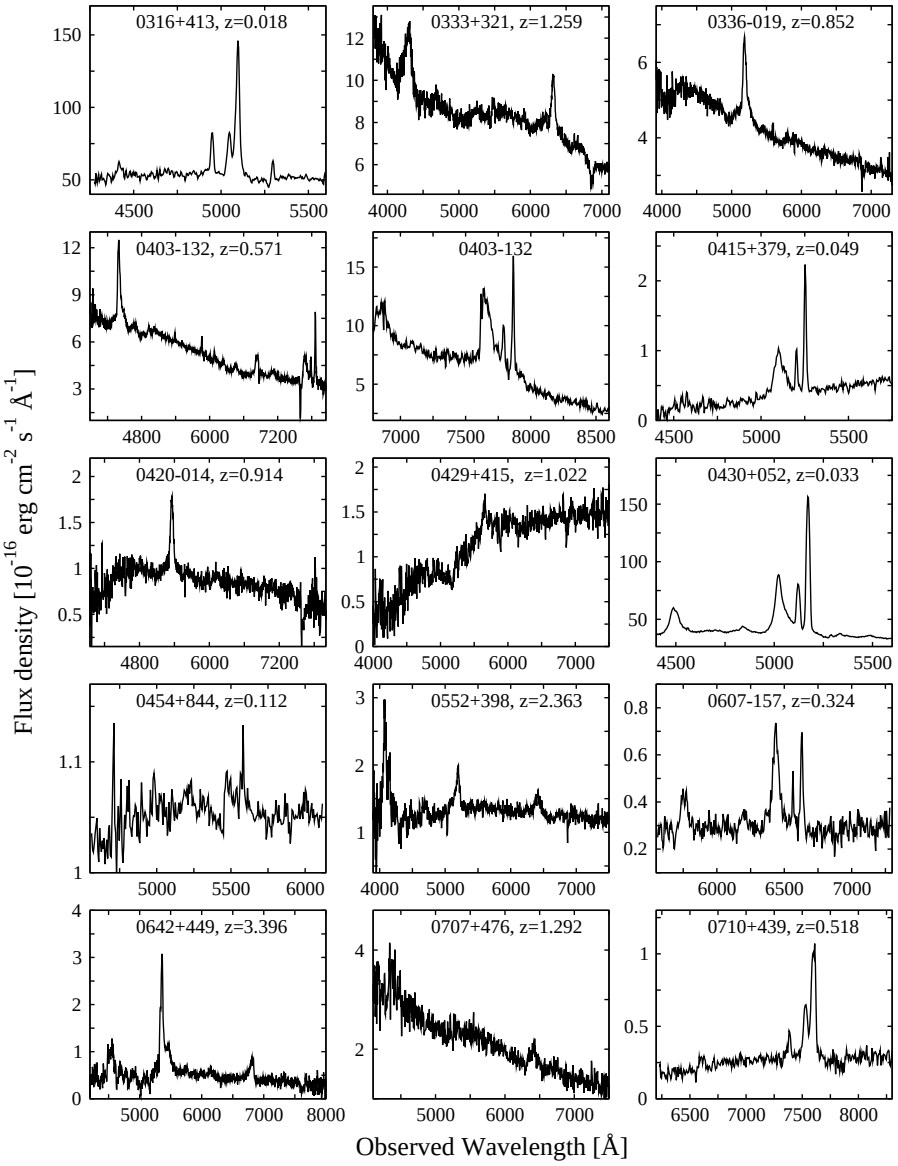

Fig. 8. (Continued)

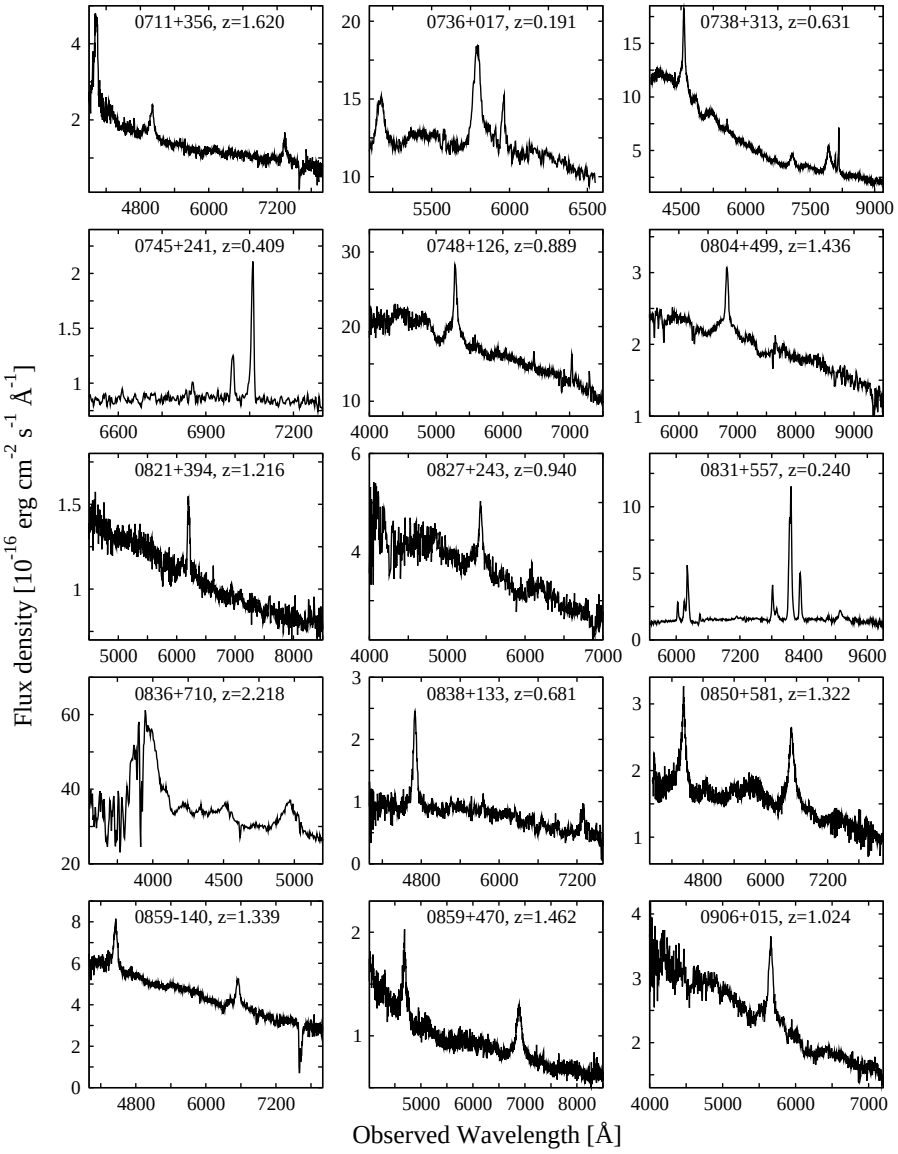

Fig. 8. (Continued)

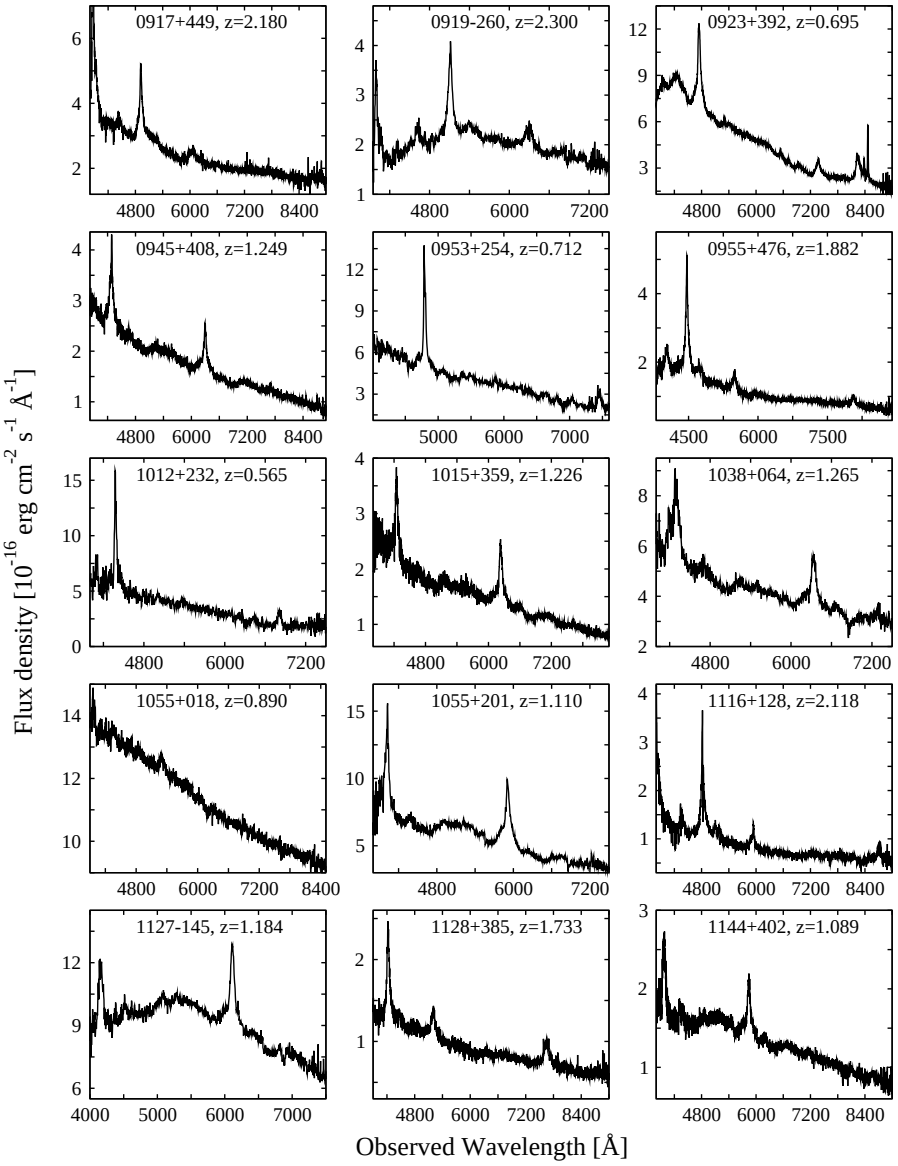

Fig. 8. (Continued)

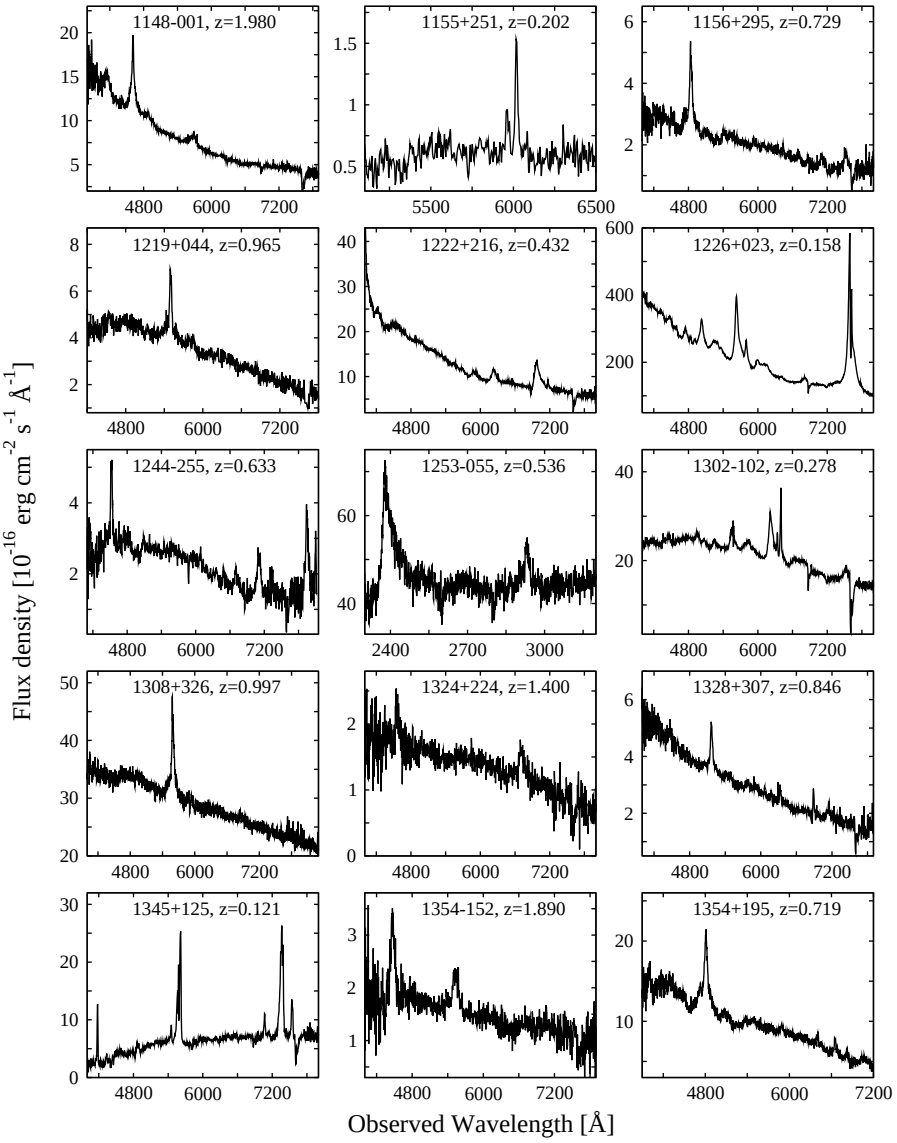

Fig. 8. (Continued)

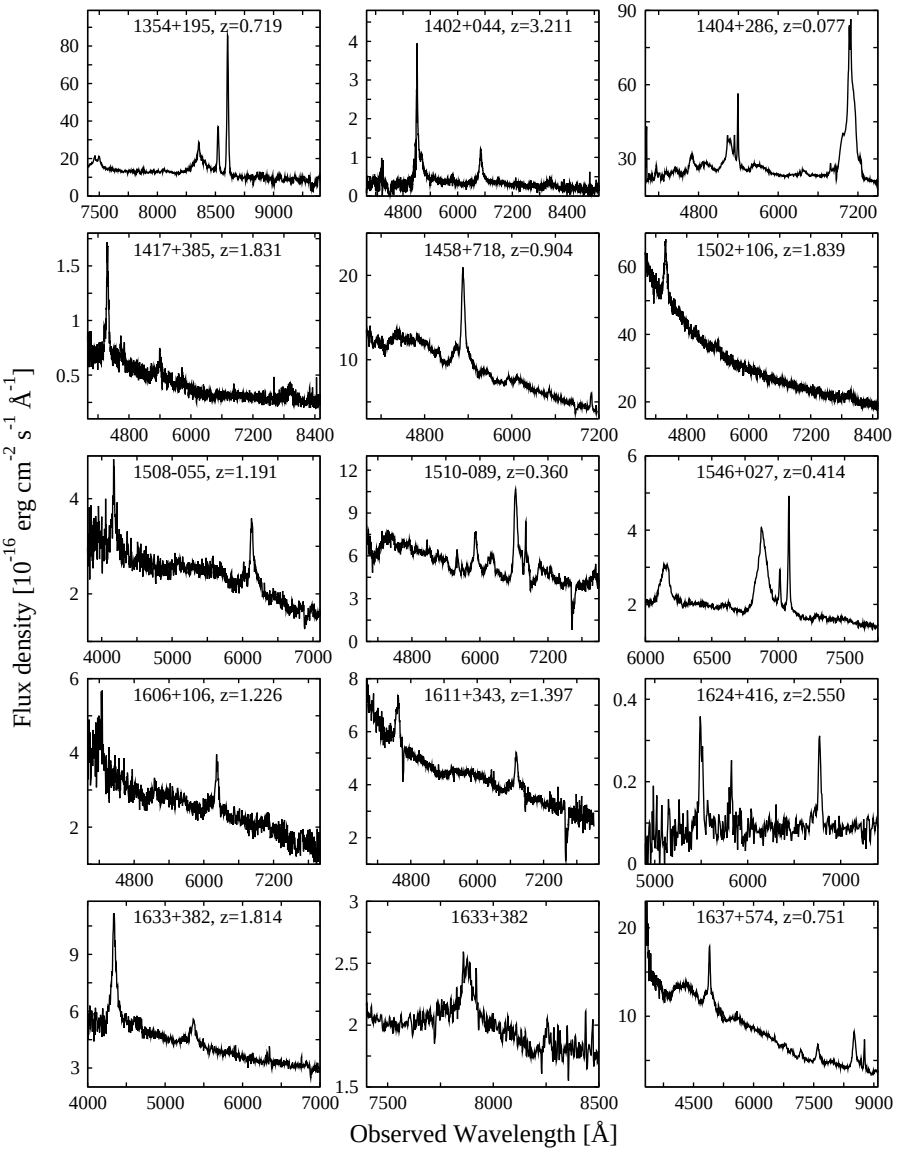

Fig. 8. (Continued)

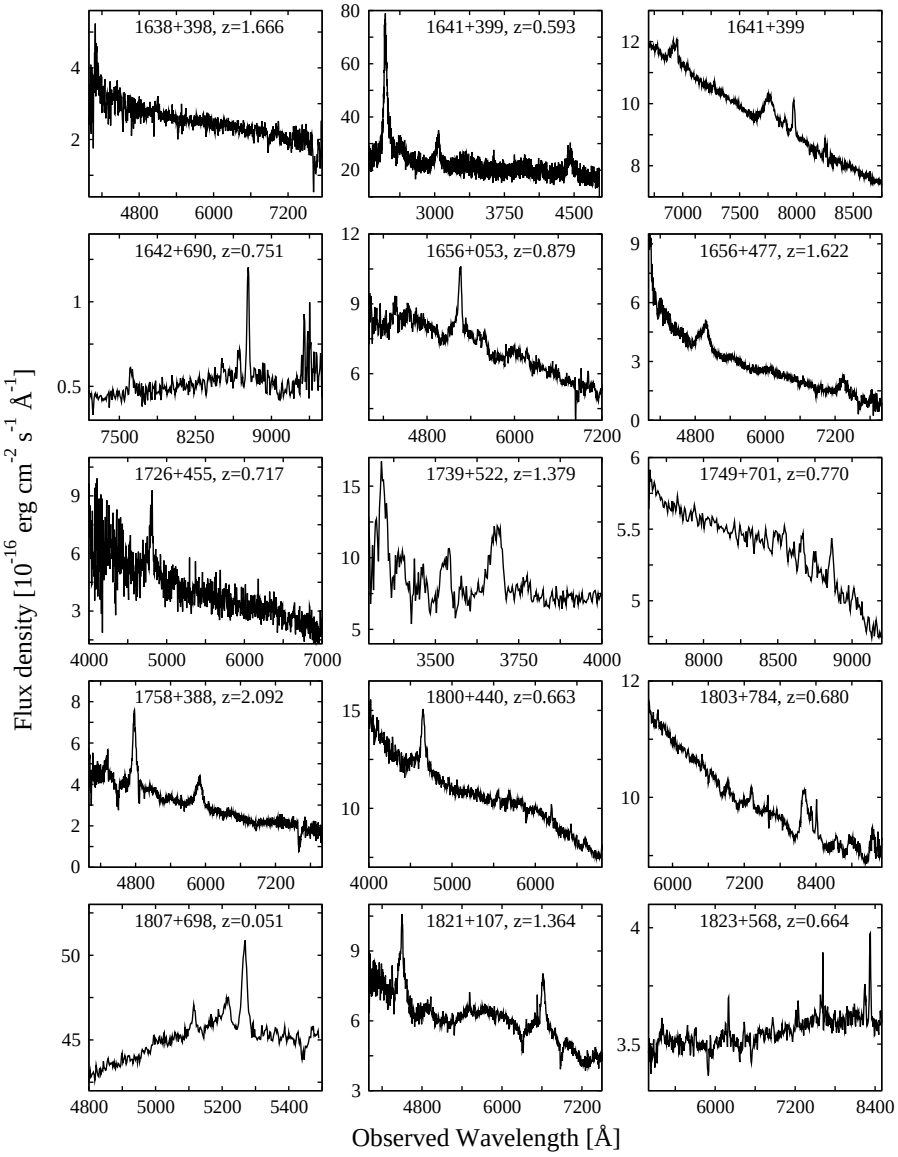

Fig. 8. (Continued)

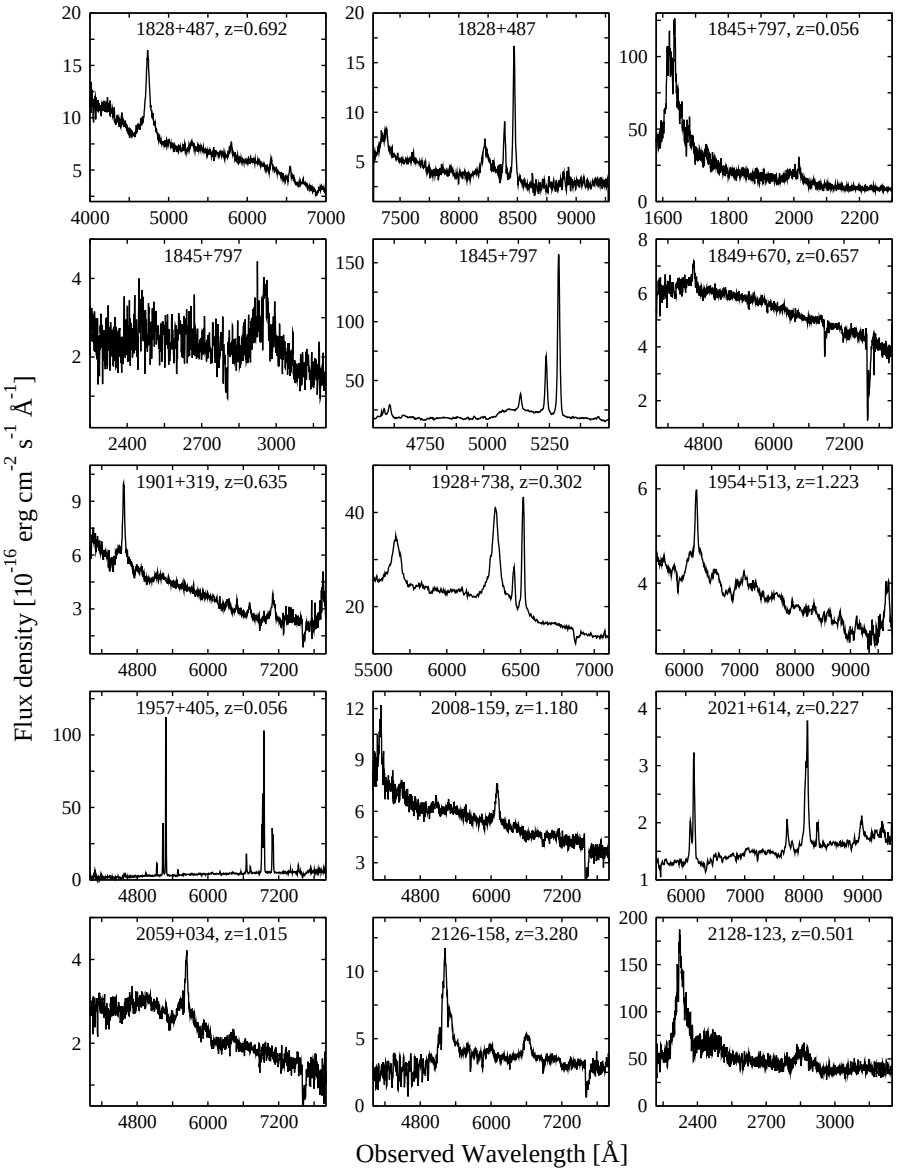

Fig. 8. (Continued)

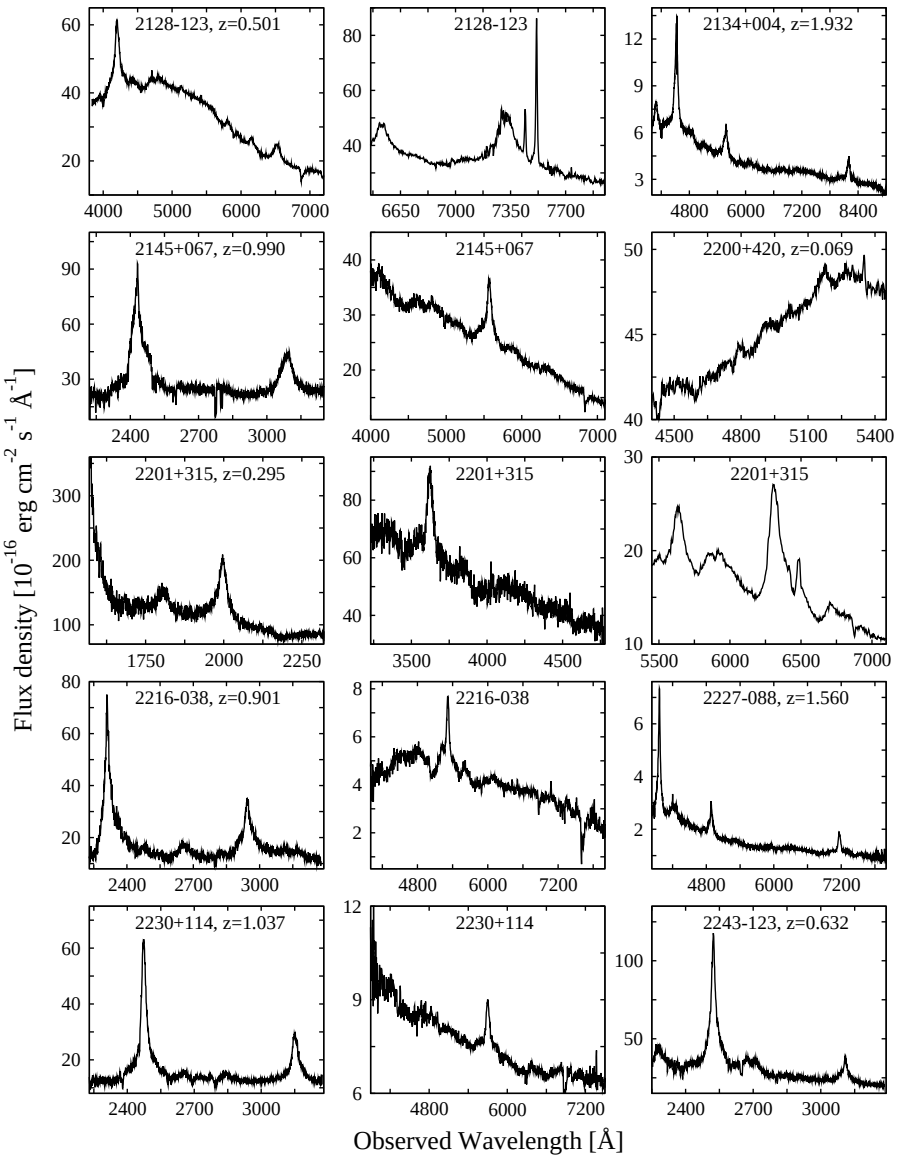

Fig. 8. (Continued)

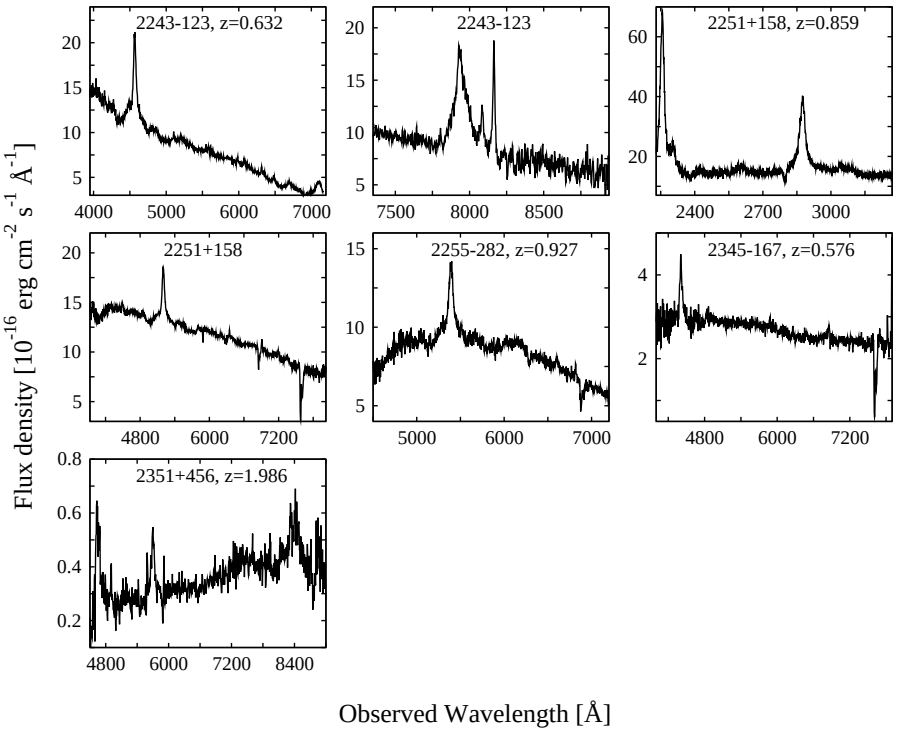

Fig. 8. (Continued)

C. SPECTROSCOPIC EMISSION LINES AND CONTINUUM PARAMETERS

TABLE 7

Hβ AND [O III] λ5007 PARAMETERS FOR 41 AGN

		Hβ (BC)				[O III] λ5007			
Source Name	Ref.[b]	FWHM (km s^{-1})	EW (Å)	Flux[c]	L_{H_β}[d]	FWHM (km s^{-1})	EW (Å)	Flux[c]	$L_{[OIII]}$[d]
0007+106	1,4	4600 ± 400	100.00 ± 6.00	151.98 ± 20.98	4.34 ± 0.60	620 ± 170	75.00 ± 20.00	105.00 ± 7.80	2.96 ± 0.22
0133+476	6	4223 ± 124	13.34 ± 0.39	3.42 ± 0.10	20.97 ± 0.61	985 ± 29	4.52 ± 0.13	1.15 ± 0.03	6.92 ± 0.20
0238−084[a]	5	1070 ± 80	10.00 ± 2.00	23.74 ± 2.00	0.001 ± 0.000	1040 ± 60	35.00 ± 3.00	65.700 ± 8.269	0.004 ± 0.001
0316+413[a]	2,4	890 ± 35	···	98.50 ± 58.70	0.13 ± 0.08	1350 ± 20	80.00 ± 50.00	359.99 ± 179.99	0.46 ± 0.23
0403−132	4	3800 ± 350	55.00 ± 5.00	37.00 ± 4.50	59.96 ± 7.29	540 ± 55	20.00 ± 3.00	11.00 ± 1.20	17.70 ± 1.93
0415+379	2	4100 ± 400	125.00 ± 15.00	4.10 ± 0.60	7.85 ± 1.15	450 ± 35	60.00 ± 10.00	2.60 ± 0.30	4.07 ± 0.47
0430+052	1,4	2750 ± 400	65.00 ± 2.00	219.96 ± 14.00	1.29 ± 0.08	450 ± 150	70.00 ± 8.00	235.00 ± 49.83	1.33 ± 0.28
0454+844	6	···	···	···	···	596 ± 5	0.64 ± 0.01	0.068 ± 0.001	0.003 ± 0.000
0607−157	2	3200 ± 450	60.00 ± 5.00	1.70 ± 0.30	1.44 ± 0.25	640 ± 130	25.00 ± 2.00	0.65 ± 0.10	0.53 ± 0.08
0710+439[a]	6	906 ± 219	21.29 ± 3.13	0.50 ± 0.07	0.67 ± 0.10	1716 ± 252	99.60 ± 14.62	2.42 ± 0.36	3.22 ± 0.47
0736+017	1	2650 ± 520	25.00 ± 5.00	28.00 ± 5.60	4.49 ± 0.90	720 ± 160	7.00 ± 2.00	8.00 ± 1.60	1.26 ± 0.25
0738+313	3	5200 ± 520	55.00 ± 5.00	18.10 ± 1.80	35.81 ± 3.56	390 ± 50	20.00 ± 2.00	3.50 ± 0.35	6.89 ± 0.69
0745+241[a]	3	370 ± 20	2.00 ± 0.30	0.01 ± 0.00	0.01 ± 0.00	370 ± 20	12.00 ± 3.00	0.98 ± 0.05	0.70 ± 0.04
0831+557[a]	6	466 ± 100	21.94 ± 1.66	3.09 ± 0.23	0.64 ± 0.05	1585 ± 120	93.74 ± 7.07	12.41 ± 0.94	2.54 ± 0.19
0923+392	3	4250 ± 400	50.00 ± 5.00	11.00 ± 3.00	25.11 ± 6.85	540 ± 50	20.00 ± 2.00	3.90 ± 0.40	8.89 ± 0.91
1155+251[a]	2	540 ± 60	8.00 ± 2.00	0.59 ± 0.06	0.07 ± 0.01	500 ± 50	65.00 ± 10.00	8.13 ± 0.80	1.02 ± 0.10
1222+216	2	5750 ± 1000	60.00 ± 15.00	37.30 ± 7.50	27.88 ± 5.61	360 ± 70	10.00 ± 3.00	2.16 ± 0.40	1.61 ± 0.30
1226+023	1,2,4	3800 ± 550	50.00 ± 7.00	1129.99 ± 99.99	85.17 ± 7.54	1300 ± 150	10.00 ± 1.00	191.00 ± 59.99	14.36 ± 4.51
1302−102	2,4	4300 ± 1000	30.00 ± 5.00	57.20 ± 3.00	16.08 ± 0.84	800 ± 15	10.00 ± 3.00	20.20 ± 0.20	5.65 ± 0.06
1345+125[a]	2	1000 ± 70	10.00 ± 2.00	5.76 ± 0.60	0.25 ± 0.03	1350 ± 120	80.00 ± 6.00	52.10 ± 5.50	2.27 ± 0.24
1354+195	4	3600 ± 310	55.00 ± 7.00	62.00 ± 13.00	178.18 ± 37.36	450 ± 60	60.00 ± 5.00	67.00 ± 6.00	191.13 ± 17.12
1404+286	1,2	8600 ± 1600	70.00 ± 6.00	148.00 ± 30.00	2.30 ± 0.47	500 ± 150	30.00 ± 2.00	43.90 ± 7.30	0.68 ± 0.11
1510−089	1,2	3250 ± 180	80.00 ± 10.00	35.50 ± 5.10	21.94 ± 3.15	550 ± 45	15.00 ± 2.00	4.90 ± 0.50	2.99 ± 0.31
1546+027	2,3	5200 ± 900	80.00 ± 2.00	15.90 ± 3.00	14.40 ± 2.72	600 ± 90	20.00 ± 3.00	4.17 ± 0.80	3.72 ± 0.71
1637+574	6	3226 ± 172	52.42 ± 2.80	20.82 ± 1.11	56.06 ± 2.99	1031 ± 55	15.50 ± 0.83	5.82 ± 0.31	15.66 ± 0.83
1641+399	3	3700 ± 190	15.00 ± 5.00	7.20 ± 0.36	10.80 ± 0.54	850 ± 40	5.00 ± 2.00	2.60 ± 0.13	3.89 ± 0.19
1642+690[a]	6	565 ± 223	9.41 ± 0.86	0.45 ± 0.04	1.32 ± 0.12	946 ± 87	23.56 ± 2.16	1.15 ± 0.11	3.37 ± 0.31
1749+701	6	···	···	···	···	1022 ± 23	1.38 ± 0.03	0.66 ± 0.01	2.01 ± 0.05

TABLE 7 (CONTINUED)

Source Name	Ref.[b]	Hβ (BC) FWHM (km s^{-1})	Hβ (BC) EW (Å)	Hβ (BC) Flux[c]	Hβ (BC) L_{H_β}[d]	[O III] λ5007 FWHM (km s^{-1})	[O III] λ5007 EW (Å)	[O III] λ5007 Flux[c]	[O III] λ5007 $L_{[OIII]}$[d]
1803+784	6	4320 ± 24	6.94 ± 0.04	6.42 ± 0.04	15.59 ± 0.09	1082 ± 6	1.56 ± 0.01	1.43 ± 0.01	3.45 ± 0.02
1807+698	6	1487 ± 16	0.88 ± 0.01	3.93 ± 0.04	0.03 ± 0.00	856 ± 9	1.86 ± 0.02	8.39 ± 0.09	0.06 ± 0.00
1823+568	6	1173 ± 18	0.46 ± 0.01	0.16 ± 0.00	0.39 ± 0.01	559 ± 9	1.66 ± 0.03	0.59 ± 0.01	1.39 ± 0.02
1828+487	4	3050 ± 340	45.00 ± 3.00	15.20 ± 2.00	42.07 ± 5.54	640 ± 60	50.00 ± 3.00	16.00 ± 2.00	43.86 ± 5.48
1845+797	4	12000 ± 1200	35.00 ± 6.00	23.00 ± 1.20	0.26 ± 0.01	580 ± 50	75.00 ± 10.00	140.00 ± 9.99	1.54 ± 0.11
1901+319	2	1670 ± 210	45.00 ± 10.00	7.22 ± 0.90	18.91 ± 2.36	500 ± 30	60.00 ± 15.00	11.70 ± 1.50	30.19 ± 3.87
1928+738	1,4	3360 ± 400	55.00 ± 2.00	85.20 ± 25.00	39.20 ± 11.50	490 ± 50	20.00 ± 1.00	29.50 ± 10.00	13.35 ± 4.53
1957+405[a]	2	560 ± 60	34.00 ± 3.00	9.78 ± 1.50	0.28 ± 0.04	550 ± 40	380.00 ± 20.00	116.00 ± 20.00	3.15 ± 0.54
2021+614	6	...	...	...	...	1394 ± 30	39.19 ± 0.83	5.08 ± 0.11	1.55 ± 0.03
2128−123	4	4900 ± 370	45.00 ± 2.00	152.00 ± 20.00	181.94 ± 23.94	370 ± 50	15.00 ± 2.00	42.00 ± 1.00	49.90 ± 1.19
2200+420	6	...	...	...	...	178 ± 2	0.24 ± 0.01	1.16 ± 0.02	0.04 ± 0.00
2201+315	1	4230 ± 300	60.00 ± 15.00	8.80 ± 1.60	3.92 ± 0.71	1200 ± 100	15.00 ± 3.00	15.00 ± 0.80	6.58 ± 0.35
2243−123	4	3900 ± 310	55.00 ± 2.00	49.60 ± 7.00	99.18 ± 14.00	490 ± 40	13.00 ± 1.00	10.50 ± 2.00	20.87 ± 3.98

[a]Source with FWHM Hβ $\lesssim$ 1000 km s^{-1}.

[b]Spectrum reference: 1=OAGH; 2=OAN-SPM; 3=*SDSS* (Sloan Digital Sky Survey); 4=Marziani et al. (2003a); 5=*HST-FOS* (Hubble Space Telescope) and 6=Lawrence et al. (1996). Values shown are mean and standard deviation for multiple spectra.

[c]Flux in units of 10^{-15} erg s^{-1} cm^{-2}.

[d]Luminosities in units of 10^{42} erg s^{-1}.

TABLE 8

PARAMETERS FOR THE λ5100 Å CONTINUUM AND FE II λ4570 FOR 41 AGN

Source	5100 Å Continuum			Fe II λ4570		
	Flux density (10^{-16} erg s^{-1} cm^{-2} Å^{-1})	λL_{5100} (10^{44} erg s^{-1})	Spectral index[a]	Flux (10^{-16} erg s^{-1} cm^{-2})	L_{4570} (10^{41} erg s^{-1})	EW (Å)
0007+106	16.10 ± 1.60	2.30 ± 0.23	−2.53	159.41 ± 0.54	4.65 ± 0.01	10.50 ± 0.67
0133+476	2.56 ± 0.07	77.63 ± 2.27	−4.44	42.90 ± 0.03	272.95 ± 0.20	16.71 ± 0.30
0238−084	17.80 ± 1.00	0.01 ± 0.00	−3.11	...	...	...
0316+413	45.00 ± 8.50	0.29 ± 0.05	−2.43	320.90 ± 0.90	0.43 ± 0.00	6.64 ± 0.35
0403−132	4.70 ± 0.40	38.40 ± 3.27	−2.67	60.29 ± 2.22	99.11 ± 3.65	7.89 ± 0.40
0415+379	0.45 ± 0.05	3.16 ± 0.35	−1.64	4.87 ± 0.02	13.94 ± 0.07	33.12 ± 10.59
0430+052	31.90 ± 3.80	0.90 ± 0.11	−2.83	273.49 ± 1.23	1.72 ± 0.01	8.21 ± 0.40
0454+844	1.04 ± 0.01	0.24 ± 0.00	−1.13	4.92 ± 0.00	0.23 ± 0.00	4.75 ± 0.07
0607−157	0.27 ± 0.03	1.11 ± 0.12	−3.89	11.24 ± 0.02	10.11 ± 0.02	50.94 ± 7.35
0710+439	0.25 ± 0.04	1.67 ± 0.24	−3.33	10.64 ± 0.01	14.50 ± 0.01	53.24 ± 5.66
0736+017	11.20 ± 2.20	8.92 ± 1.75	−1.16	204.70 ± 0.17	33.88 ± 0.03	18.20 ± 0.32
0738+313	2.56 ± 0.30	25.59 ± 3.00	−2.55	85.67 ± 0.02	171.52 ± 0.05	28.28 ± 0.93
0745+241	0.83 ± 0.03	3.04 ± 0.11	−0.86	3.03 ± 0.02	2.23 ± 0.01	3.54 ± 0.16
0831+557	1.32 ± 0.10	1.37 ± 0.10	−3.26	16.23 ± 0.10	3.37 ± 0.01	13.63 ± 0.69
0923+392	1.93 ± 0.20	22.41 ± 2.32	−1.75	11.52 ± 0.02	26.35 ± 0.05	4.93 ± 0.20
1155+251	1.27 ± 0.13	0.81 ± 0.08	−5.10	28.13 ± 0.05	3.56 ± 0.01	64.36 ± 9.92
1222+216	6.84 ± 0.31	25.96 ± 1.18	−0.83	...	...	...
1226+023	218.00 ± 40.00	83.45 ± 15.31	−2.08	4520.37 ± 29.91	342.38 ± 2.26	13.59 ± 0.67
1302−102	19.20 ± 1.00	27.30 ± 1.42	−2.27	186.77 ± 0.54	53.13 ± 0.13	9.81 ± 0.25
1345+125	5.72 ± 0.23	1.27 ± 0.05	−2.49	100.65 ± 0.19	4.45 ± 0.01	27.46 ± 1.40
1354+195	9.80 ± 0.90	141.91 ± 13.03	−2.61	60.12 ± 0.54	175.28 ± 1.41	4.82 ± 0.26
1404+286	21.80 ± 2.40	1.72 ± 0.19	−2.59	449.82 ± 0.54	7.02 ± 0.01	20.47 ± 0.76
1510−089	3.86 ± 0.25	11.94 ± 0.77	−3.20	270.95 ± 0.25	171.50 ± 0.16	68.72 ± 8.58
1546+027	2.00 ± 0.50	9.01 ± 2.26	−1.52	28.36 ± 0.08	26.45 ± 0.08	15.50 ± 2.26
1637+574	3.56 ± 0.19	48.81 ± 2.61	−0.60	47.53 ± 0.07	128.41 ± 0.18	10.69 ± 0.31
1641+399	11.40 ± 0.20	86.95 ± 1.53	−3.14	18.53 ± 0.30	27.83 ± 0.45	1.79 ± 0.04
1642+690	0.53 ± 0.05	7.87 ± 0.72	−2.82	7.00 ± 0.00	20.77 ± 0.01	15.72 ± 1.03
1749+701	4.92 ± 0.11	76.20 ± 1.72	−1.30	17.88 ± 0.02	55.11 ± 0.05	3.29 ± 0.04

TABLE 8 (CONTINUED)

Source	5100 Å Continuum			Fe II λ4570		
	Flux density (10^{-16} erg s^{-1} cm^{-2} Å^{-1})	λL_{5100} (10^{44} erg s^{-1})	Spectral index[a]	Flux (10^{-16} erg s^{-1} cm^{-2})	L_{4570} (10^{41} erg s^{-1})	EW (Å)
1803+784	9.13 ± 0.05	111.91 ± 0.61	−2.05	19.41 ± 0.11	47.72 ± 0.26	2.02 ± 0.03
1807+698	44.82 ± 0.47	1.59 ± 0.02	−2.23	362.20 ± 0.37	2.55 ± 0.00	9.00 ± 0.16
1823+568	3.56 ± 0.05	42.42 ± 0.65	−0.15	17.73 ± 0.00	42.50 ± 0.01	5.07 ± 0.13
1828+487	2.52 ± 0.30	35.02 ± 4.17	−3.61	46.79 ± 0.30	131.98 ± 0.85	10.59 ± 1.37
1845+797	17.50 ± 1.00	0.98 ± 0.06	−8.86	296.66 ± 0.31	3.35 ± 0.00	18.51 ± 0.96
1901+319	2.18 ± 0.30	28.42 ± 3.91	−2.25	77.17 ± 0.36	208.24 ± 0.98	38.84 ± 3.58
1928+738	12.80 ± 5.30	29.25 ± 12.11	−2.12	205.07 ± 0.54	97.43 ± 0.26	9.29 ± 0.46
1957+405	1.80 ± 0.39	0.24 ± 0.05	−2.53	138.58 ± 0.22	4.35 ± 0.01	85.74 ± 12.31
2021+614	1.28 ± 0.03	1.96 ± 0.04	−2.41	6.27 ± 0.02	2.07 ± 0.01	5.08 ± 0.33
2128−123	30.00 ± 1.00	180.90 ± 6.03	−0.68	...	...	...
2200+420	47.21 ± 0.63	8.28 ± 0.11	−2.70	205.61 ± 0.20	8.20 ± 0.01	4.73 ± 0.07
2201+315	12.00 ± 1.00	26.59 ± 2.22	−1.07	232.43 ± 0.25	106.49 ± 0.12	13.29 ± 0.31
2243−123	7.27 ± 0.80	73.41 ± 8.08	−1.96	...	...	...

[a]Spectral index of the local continuum power-law.

TABLE 9

PARAMETERS FOR THE 3000 Å CONTINUUM AND MG II λ2798 FOR 78 AGN

		Mg II (BC)				3000 Å, Continuum		
Source	Ref[a]	FWHM ($km\,s^{-1}$)	EW (Å)	Flux[b]	$L_{Mg\,II}$ (10^{42} $erg\,s^{-1}$)	Flux[c]	λL_{3000} (10^{44} $erg\,s^{-1}$)	Spectral index[d]
0007+106	5	6322 ± 635	57.69 ± 5.80	256.10 ± 25.74	9.06 ± 0.91	42.84 ± 4.31	4.35 ± 0.44	−0.90
0016+731	6	4989 ± 132	20.60 ± 3.33	3.72 ± 0.10	498.72 ± 13.38	1.39 ± 0.06	484.93 ± 19.22	−0.09
0112−017	2	5304 ± 777	40.53 ± 5.94	1.33 ± 0.19	21.16 ± 3.09	0.29 ± 0.04	13.47 ± 1.97	−0.30
0113−118	2	4751 ± 42	70.57 ± 0.83	17.06 ± 1.63	39.35 ± 3.75	2.50 ± 0.36	17.04 ± 2.45	−0.23
0122−003	2	5140 ± 491	37.30 ± 1.69	16.90 ± 0.58	127.30 ± 4.37	4.05 ± 0.26	90.22 ± 5.88	−0.85
0133−203	2	5072 ± 648	74.43 ± 9.51	6.00 ± 0.77	48.28 ± 6.17	0.95 ± 0.12	22.76 ± 2.90	−1.09
0133+476	2	5367 ± 453	46.26 ± 3.90	3.27 ± 0.28	28.10 ± 2.37	0.73 ± 0.06	17.68 ± 1.49	−2.62
0202+319	2	4271 ± 467	34.86 ± 3.81	2.67 ± 0.29	50.61 ± 5.53	0.69 ± 0.08	38.39 ± 4.20	−2.73
0248+430	2	5560 ± 442	37.77 ± 3.00	10.69 ± 0.85	201.10 ± 15.97	2.98 ± 0.24	160.17 ± 12.74	−9.65
0310+013	2	4808 ± 396	79.49 ± 17.60	4.65 ± 0.27	21.18 ± 1.23	0.81 ± 0.15	10.29 ± 1.98	−7.88
0333+321	1	3735 ± 272	14.60 ± 1.06	9.03 ± 0.66	6091.17 ± 443.18	5.67 ± 0.41	8205.02 ± 597.65	−0.61
0336−019	2	4781 ± 958	22.85 ± 3.45	9.15 ± 1.16	52.68 ± 6.68	3.88 ± 0.06	64.45 ± 0.96	−0.15
0403−132	2,5	4752 ± 138	41.36 ± 13.45	23.64 ± 5.15	43.52 ± 9.50	6.11 ± 0.26	32.85 ± 1.43	−1.35
0420−014	2	4846 ± 65	73.72 ± 0.99	4.82 ± 0.06	43.37 ± 0.58	7.70 ± 0.10	196.00 ± 2.65	−6.70
0429+415	2	5757 ± 19	33.46 ± 7.69	3.14 ± 0.59	421.56 ± 78.54	1.23 ± 0.06	386.04 ± 19.97	−3.47
0707+476	2	6849 ± 522	32.02 ± 2.44	4.20 ± 0.32	64.75 ± 4.93	1.40 ± 0.11	62.50 ± 4.78	−0.76
0711+356	2	3908 ± 657	33.92 ± 5.70	2.56 ± 0.43	61.02 ± 10.27	0.68 ± 0.11	47.33 ± 7.95	−0.75
0738+313	3	5357 ± 181	39.69 ± 1.34	36.43 ± 1.23	80.13 ± 2.71	8.38 ± 0.28	54.20 ± 1.83	−0.50
0748+126	2	5297 ± 194	26.29 ± 0.96	41.90 ± 1.53	195.69 ± 7.15	15.87 ± 0.58	219.74 ± 8.02	−3.56
0804+499	6	7495 ± 323	11.79 ± 1.55	2.84 ± 0.11	48.75 ± 1.85	1.91 ± 0.06	96.07 ± 3.11	−0.12
0821+394	3	2445 ± 82	10.73 ± 0.36	1.13 ± 0.04	12.43 ± 0.42	0.97 ± 0.03	31.23 ± 1.05	−0.97
0827+243	2	5304 ± 209	22.67 ± 0.89	7.15 ± 0.28	38.78 ± 1.53	3.09 ± 0.12	49.54 ± 1.96	−0.11
0838+133	2	4683 ± 427	78.99 ± 7.20	6.35 ± 0.58	21.96 ± 2.00	0.79 ± 0.07	7.83 ± 0.71	−0.58
0850+581	3	5359 ± 318	53.09 ± 3.15	6.79 ± 0.40	95.81 ± 5.69	1.17 ± 0.07	48.36 ± 2.88	−3.31
0859−140	2,1	4996 ± 268	22.95 ± 8.65	7.81 ± 2.47	117.91 ± 37.29	3.18 ± 0.20	140.08 ± 8.85	−0.22
0859+470	3	5252 ± 282	42.70 ± 2.29	2.99 ± 0.16	44.72 ± 2.39	0.68 ± 0.04	30.11 ± 1.61	−3.16
0906+015	3,2	4616 ± 43	28.70 ± 5.97	7.18 ± 0.81	47.64 ± 5.40	2.39 ± 0.75	46.88 ± 14.81	−1.01
0923+392	3	4927 ± 247	52.59 ± 2.63	30.95 ± 1.55	73.05 ± 3.65	5.58 ± 0.28	39.20 ± 1.96	−0.12
0945+408	2,3	5116 ± 307	40.57 ± 6.24	4.82 ± 0.05	47.35 ± 0.53	1.13 ± 0.19	33.09 ± 5.62	−2.36
0953+254	2	4006 ± 1434	42.31 ± 0.28	12.77 ± 8.80	35.45 ± 24.38	2.82 ± 1.86	23.05 ± 15.21	−1.77
1012+232	2	3381 ± 314	70.34 ± 6.53	28.22 ± 2.62	42.72 ± 3.97	3.85 ± 0.36	17.31 ± 1.60	−0.15
1015+359	3	4100 ± 196	36.07 ± 1.72	4.44 ± 0.21	41.36 ± 1.97	1.12 ± 0.05	31.14 ± 1.48	−1.13

TABLE 9 (CONTINUED)

		Mg II (BC)				3000 Å, Continuum		
Source	Ref[a]	FWHM ($km\,s^{-1}$)	EW (Å)	Flux[b]	$L_{Mg\,II}$ (10^{42} $erg\,s^{-1}$)	Flux[c]	λL_{3000} (10^{44} $erg\,s^{-1}$)	Spectral index[d]
1038+064	2	4696 ± 317	42.39 ± 2.86	12.27 ± 0.83	132.42 ± 8.91	2.83 ± 0.19	90.40 ± 6.10	−2.58
1055+018	3	6039 ± 130	5.83 ± 0.13	7.46 ± 0.16	34.07 ± 0.73	12.60 ± 0.27	170.56 ± 3.65	−1.64
1055+201	2	6208 ± 404	53.79 ± 3.50	22.62 ± 1.47	175.83 ± 11.44	3.88 ± 0.25	89.57 ± 5.84	−0.72
1116+128	3	4054 ± 272	33.29 ± 2.23	1.50 ± 0.10	58.32 ± 3.93	0.44 ± 0.03	50.75 ± 3.40	−2.95
1127−145	2	5101 ± 190	26.76 ± 5.06	19.57 ± 4.52	194.05 ± 44.75	7.14 ± 0.52	208.63 ± 15.28	−0.12
1128+385	3	5543 ± 432	35.84 ± 2.79	2.15 ± 0.17	50.26 ± 3.93	0.60 ± 0.05	41.95 ± 3.27	−1.16
1144+402	3	4822 ± 237	32.13 ± 1.58	3.88 ± 0.19	27.70 ± 1.36	1.19 ± 0.06	25.29 ± 1.25	−0.69
1156+295	2	4245 ± 225	50.36 ± 2.66	10.74 ± 0.57	28.77 ± 1.53	2.05 ± 0.11	16.39 ± 0.87	−1.16
1219+044	2	5268 ± 335	16.56 ± 4.37	7.36 ± 0.52	39.40 ± 2.77	3.17 ± 0.14	50.46 ± 2.26	−0.46
1244−255	2	2565 ± 713	8.30 ± 3.55	2.61 ± 0.69	7.28 ± 1.92	2.52 ± 0.14	20.28 ± 1.10	−0.09
1308+326	3	5267 ± 360	11.12 ± 1.73	3.81 ± 0.22	21.33 ± 1.25	2.81 ± 0.09	46.91 ± 1.43	0.00
1324+224	2	5129 ± 317	36.83 ± 10.38	4.38 ± 0.24	57.85 ± 3.21	0.79 ± 0.15	31.23 ± 6.06	−1.18
1328+307	2	3378 ± 119	16.56 ± 0.58	5.32 ± 0.19	19.88 ± 0.70	2.99 ± 0.11	33.34 ± 1.18	−0.68
1354+195	1	5321 ± 245	47.39 ± 2.18	44.12 ± 2.03	144.17 ± 6.64	9.07 ± 0.42	86.59 ± 3.99	−0.08
1417+385	3	4287 ± 739	31.93 ± 5.50	0.71 ± 0.12	17.23 ± 2.98	0.25 ± 0.04	17.89 ± 3.08	−3.48
1458+718	1	5131 ± 77	48.26 ± 0.83	31.94 ± 6.84	152.67 ± 32.74	6.15 ± 1.49	87.30 ± 21.15	−1.89
1508−055	1,2	6216 ± 159	40.71 ± 3.01	8.87 ± 3.54	113.37 ± 45.25	2.24 ± 0.85	82.69 ± 31.56	−2.23
1606+106	2	5012 ± 307	18.85 ± 4.20	5.04 ± 0.31	62.29 ± 3.83	2.01 ± 0.13	72.47 ± 4.69	−2.93
1611+343	2	5561 ± 271	23.74 ± 1.16	7.48 ± 0.36	99.46 ± 4.84	3.09 ± 0.15	122.28 ± 5.94	−2.57
1633+382	3	5583 ± 323	18.77 ± 1.09	3.25 ± 0.19	78.33 ± 4.53	1.70 ± 0.10	122.31 ± 7.06	−2.57
1637+574	6	3899 ± 136	29.69 ± 1.03	28.72 ± 1.00	79.50 ± 2.77	8.57 ± 0.30	70.82 ± 2.46	−1.48
1641+399	1,5	5520 ± 1135	46.44 ± 7.20	66.16 ± 6.61	102.18 ± 10.20	15.23 ± 0.94	69.97 ± 4.34	−1.75
1656+053	2	4748 ± 133	18.41 ± 0.52	12.58 ± 0.35	121.93 ± 3.42	6.73 ± 0.19	182.04 ± 5.11	−0.60
1656+477	2	6824 ± 1203	77.86 ± 39.91	11.39 ± 4.33	222.05 ± 84.34	0.64 ± 0.25	36.76 ± 14.65	−3.35
1726+455	1	5771 ± 934	176.80 ± 28.63	32.42 ± 5.25	84.83 ± 13.75	3.37 ± 0.54	26.18 ± 4.23	−5.60
1800+440	1	4659 ± 837	13.05 ± 2.66	15.31 ± 3.65	40.79 ± 9.73	11.32 ± 4.77	87.94 ± 6.51	−0.94
1821+107	2	5265 ± 152	22.55 ± 4.36	13.30 ± 0.38	438.47 ± 12.59	4.19 ± 0.84	380.80 ± 15.90	−1.16
1828+487	2	5427 ± 143	27.42 ± 0.72	29.04 ± 0.77	95.07 ± 2.52	9.97 ± 0.26	94.74 ± 2.50	−2.48
1845+797	5	6874 ± 275	44.00 ± 13.62	11.08 ± 0.44	0.14 ± 0.01	1.26 ± 0.31	0.05 ± 0.01	−4.02
1849+670	2	5868 ± 156	15.00 ± 0.40	8.13 ± 0.22	20.85 ± 0.55	5.83 ± 0.15	43.73 ± 1.16	−0.53
1901+319	1,2	5099 ± 491	30.56 ± 6.53	12.90 ± 0.15	44.93 ± 0.52	4.04 ± 0.85	39.99 ± 8.46	−2.88
1954+513	6	8752 ± 354	15.14 ± 1.86	7.28 ± 0.30	147.80 ± 6.15	3.84 ± 0.11	218.69 ± 6.44	−0.15
2008−159	2	4955 ± 219	15.72 ± 2.65	9.10 ± 0.41	161.02 ± 7.31	4.48 ± 0.14	223.21 ± 7.12	−3.18
2059+034	2	4731 ± 260	37.13 ± 2.04	7.54 ± 0.41	73.44 ± 4.04	1.93 ± 0.11	53.85 ± 2.96	−0.87
2128−123	1	5282 ± 131	27.79 ± 0.69	109.50 ± 2.72	150.67 ± 3.73	40.32 ± 1.00	161.12 ± 4.00	−2.44

TABLE 9 (CONTINUED)

		Mg II (BC)				3000 Å, Continuum		
Source	Ref[a]	FWHM ($km\,s^{-1}$)	EW (Å)	Flux[b]	$L_{Mg\,II}$ (10^{42} $erg\,s^{-1}$)	Flux[c]	λL_{3000} (10^{44} $erg\,s^{-1}$)	Spectral index[d]
2134+004	3	5194 ± 351	24.91 ± 1.68	6.13 ± 0.41	235.34 ± 15.89	2.33 ± 0.16	260.67 ± 17.56	−2.42
2145+067	1	5517 ± 152	25.20 ± 0.70	56.88 ± 1.57	457.53 ± 12.62	21.34 ± 0.59	495.82 ± 13.71	−0.47
2201+315	5	5248 ± 308	36.96 ± 2.17	184.70 ± 10.85	108.11 ± 6.37	47.88 ± 2.81	79.47 ± 4.66	−2.37
2216−038	2	6198 ± 287	25.23 ± 1.17	10.14 ± 0.47	70.04 ± 3.26	3.94 ± 0.18	78.57 ± 3.63	−0.31
2227−088	3	5896 ± 322	18.75 ± 1.03	1.81 ± 0.10	38.15 ± 2.09	0.92 ± 0.05	56.98 ± 3.11	−3.71
2230+114	2	4583 ± 77	11.80 ± 0.20	8.19 ± 0.14	71.21 ± 1.19	6.65 ± 0.11	167.96 ± 2.80	−3.53
2243−123	1	5838 ± 411	31.84 ± 0.63	29.74 ± 2.74	66.25 ± 6.11	8.75 ± 0.66	57.27 ± 4.34	−2.53
2251+158	1,2	5162 ± 473	14.94 ± 1.08	19.01 ± 2.28	125.98 ± 15.12	12.50 ± 1.77	237.05 ± 33.57	−3.84
2255−282	1	5171 ± 190	26.32 ± 0.96	21.64 ± 0.79	113.03 ± 4.15	8.39 ± 0.31	129.76 ± 4.76	−2.82
2345−167	2	4678 ± 222	26.07 ± 1.24	6.73 ± 0.32	10.72 ± 0.51	2.76 ± 0.13	13.04 ± 0.62	−4.83
2351+456	6	6266 ± 656	36.88 ± 10.50	1.74 ± 0.34	99.19 ± 19.44	0.33 ± 0.06	54.25 ± 9.10	0.64

[a]Spectrum reference: 1=OAGH; 2=OAN-SPM; 3=*SDSS* (Sloan Digital Sky Survey); 4=Marziani et al. (2003a); 5=*HST-FOS* (Hubble Space Telescope) y 6=Lawrence et al. (1996). Values shown are the mean and standard deviation if multiple spectra were available.
[b]Flux in units of 10^{-15} $erg\,s^{-1}\,cm^{-2}$
[c]Flux density in units of 10^{-16} $erg\,s^{-1}\,cm^{-2}\,Å^{-1}$
[d]Spectral index of local continuum power-law.

TABLE 10

FE II λ2490 PARAMETERS FOR 78 AGN

	Fe II λ2490[a]					Fe II λ2490[a]			
Source	Flux[b]	L_{2490}[c]	EW (Å)	λ_{Fe}[d]	Source	Flux[b]	L_{2490}[c]	EW (Å)	λ_{Fe}[d]
0007+106	405.42±1.55	16.09±0.06	67.05±6.74		1156+295	18.70±0.05	51.45±0.14	59.54±3.15	2300
0016+731	8.10 ±0.00	1584.21±0.72	50.30±8.13		1219+044	38.21±0.03	209.30 ±0.16	79.30±20.91	
0112−017	4.12 ±0.01	70.54±0.22	75.50±11.06		1244−255	23.57±0.02	72.94±0.05	70.27±30.05	2436
0113−118	···	···	···		1308+326	10.14±0.02	57.49±0.09	30.17±4.68	
0122−003	36.24±0.03	283.20±0.25	56.66±2.57		1324+224	17.03±0.00	229.03±0.04	110.16±31.04	
0133−203	19.75±0.05	161.82±0.39	120.59±15.40		1328+307	···	···	···	
0133+476	3.84 ±0.01	39.52±0.09	46.02±3.88		1354+195	106.32±0.24	372.16±0.83	76.87±3.54	
0202+319	7.81 ±0.02	158.72±0.31	64.38±7.04		1417+385	1.86 ±0.01	45.90±0.12	54.91±9.46	
0248+430	29.82±0.06	635.95±1.36	78.69±6.26		1458+718	68.40±0.18	337.40 ±0.88	67.07±1.15	
0310+013	···	···	···		1508−055	25.65±0.07	361.88±0.92	76.59±5.67	
0333+321	53.76±0.11	88402±176	62.54±4.55		1606+106	15.67±0.01	208.97±0.06	55.75±12.43	
0336−019	15.35±0.03	97.69±0.18	30.68±4.63		1611+343	20.85±0.07	283.83±0.92	47.51±2.32	
0403−132	60.01±0.09	118.27±0.18	75.31±24.49		1633+382	7.56 ±0.02	184.62±0.45	34.26±1.98	
0420−014	4.83 ±0.01	50.77±0.10	6.20 ±0.08		1637+574	56.15±0.21	157.73 ±0.60	19.61±0.68	
0429+415	10.59±0.02	2759.66±4.87	97.16±22.32		1641+399	124.33±0.32	194.42±0.50	58.40±9.05	
0707+476	5.25±0.02	88.91±0.29	24.53±1.87		1656+053	38.62±0.09	450.67±1.05	45.80±1.29	
0711+356	5.52±0.01	140.76±0.33	47.09±7.91		1656+477	19.49±0.01	389.42±0.14	91.67±46.99	
0738+313	35.62±0.12	82.83±0.28	28.05±0.95	2340	1726+455	74.74±0.24	201.30±0.64	111.20±18.00	2190
0748+126	89.89±0.25	435.49±1.21	44.52±1.63		1800+440	33.17±0.11	95.15±0.31	21.80±4.44	
0804+499	9.37±0.00	171.24±0.07	40.11±5.26	2245	1821+107	44.50±0.01	1836.31±0.58	70.62±13.65	
0821+394	2.64±0.01	30.64±0.07	21.19±0.71		1828+487	27.91±0.15	100.22±0.54	18.48±0.49	2360
0827+243	20.29±0.05	114.47±0.28	48.26±1.90		1845+797	29.54±0.07	0.42±0.00	115.13±35.65	
0838+133	···	···	···	2300	1849+670	···	···	···	2400
0850+581	12.81±0.03	192.49±0.44	73.75±4.38		1901+319	22.03±0.08	88.45±0.33	40.87±8.74	
0859−140	15.40±0.04	250.31±0.61	34.21±12.90		1954+513	11.49±0.01	279.08±0.30	26.10±3.20	2475
0859+470	4.18±0.01	63.99±0.16	44.29±2.37		2008−159	21.64±0.01	452.22±0.25	36.13±6.09	
0906+015	13.94±0.04	96.12±0.26	40.70±8.46		2059+034	24.31±0.06	267.56±0.66	82.07±4.52	
0923+392	53.89±0.14	129.20±0.35	63.23±3.16	2236	2128−123	···	···	···	2500
0945+408	10.22±0.03	101.86±0.27	56.87±8.74		2134+004	15.86±0.05	659.36±1.95	45.64±3.09	
0953+254	12.47±0.05	36.16±0.15	36.00±0.23		2145+067	116.37±0.31	1025.39±2.77	37.93±1.05	
1012+232	···	···	···	2558	2201+315	···	···	···	2490

TABLE 10 (CONTINUED)

	Fe II λ2490[a]					Fe II λ2490[a]			
Source	Flux[b]	L_{2490}[c]	EW (Å)	λ_{Fe}[d]	Source	Flux[b]	L_{2490}[c]	EW (Å)	λ_{Fe}[d]
1015+359	8.93±0.03	84.33±0.31	52.18±2.49		2216−038	37.04±0.10	287.05±0.74	71.84±3.33	
1038+064	29.15±0.07	322.63±0.82	67.30±4.54		2227−088	4.29±0.01	96.08±0.32	33.39±1.83	
1055+018	18.34±0.06	86.27±0.28	12.35±0.27		2230+114	14.26±0.05	135.46±0.51	17.61±0.30	
1055+201	38.59±0.09	309.18±0.75	61.79±4.02		2243−123	36.74±0.14	86.85±0.32	30.31±0.60	
1116+128	4.16±0.01	166.66±0.41	60.91±4.08		2251+158	36.58±0.11	275.48±0.83	24.98±1.80	
1127−145	50.37±0.11	521.09±1.13	52.36±9.91		2255−282	59.92±0.12	326.19±0.63	66.88±2.45	
1128+385	4.36±0.01	105.02±0.26	50.39±3.92		2345−167	···	···	···	2450
1144+402	10.39±0.04	75.79±0.27	62.73±3.08		2351+456	5.30±0.00	349.14±0.12	127.57±36.31	

[a]Fe II λ2490 corresponds to the Fe II emission in the 2180-2800 Å spectral region.
[b]Flux in units of 10^{-15} erg s^{-1} cm^{-2}.
[c]Luminosity in units of 10^{42} erg s^{-1}
[d]Lower value of wavelength (Å) at which spectra allowed the measurement of Fe II λ2490 emission. If omitted, the value is 2180 Å.

TABLE 11

C IV λ1549 AND CONTINUUM AT 1350 Å FOR 35 AGN

		C IV (BC)				Continuum 1350 Å		
Name	Ref[a]	FWHM ($km\,s^{-1}$)	EW (Å)	Flux[b]	$L_{C\,IV}$ (10^{42} $erg\,s^{-1}$)	Flux[c]	λL_{1350} (10^{44} $erg\,s^{-1}$)	Spectral index[d]
0016+731	6	7906±952	22.78±2.74	2.91±0.35	705.03±85.04	1.45±0.12	594.71±49.63	...
0153+744	1	6220±655	22.36±2.35	3.14±0.33	5188.08±546.90	1.10±0.18	3460.14±556.77	−6.30
0212+735	6	5579±408	10.48±0.77	0.94±0.07	11345.32±829.08	0.70±0.11	19565.88±2997.33	−1.85
0552+398	2	4352±334	10.42±0.80	1.29±0.10	1462.35±112.00	1.22±0.11	2536.05±234.9	−8.12
0642+449	2	4025±1652	24.91±5.44	1.06±0.45	258.23±109.04	0.65±0.18	232.9±63.24	−1.60
0711+356	2	4941±257	27.64±1.44	6.03±0.31	159.76±8.32	2.69±0.14	100.19±5.21	−2.34
0836+710	1,6	7657±130	13.27±0.33	23.71±16.67	1111.15±782.39	23.00±15.90	1487.7±1024.52	−1.17
0917+449	3	6935±436	17.61±1.11	4.96±0.31	206.76±13.01	3.35±0.17	191.31±9.48	−0.95
0919−260	2	4895±390	15.77±1.26	3.42±0.27	380.03±30.22	1.90±0.22	313.24±36.93	−15.68
0955+476	3	5673±649	36.28±4.15	5.88±0.67	161.82±18.52	1.84±0.26	69.08±9.65	−1.06
1116+128	3	6514±1217	37.14±6.94	3.86±0.72	155.31±29.01	1.25±0.17	69.13±9.46	−3.82
1128+385	3	7343±821	22.46±2.51	2.67±0.30	65.69±7.36	1.57±0.11	53.09±3.55	−0.40
1148−001	2	6198±43	13.79±2.74	12.30±1.44	409.67±47.10	11.48±4.60	523.65±209.37	−1.84
1253−055	5	8613±350	25.68±6.54	18.88±1.87	26.61±2.63	38.44±9.79	74.48±18.99	7.20
1354−152	2	8505±2066	35.13±8.53	5.47±1.33	280.23±68.14	1.65±0.40	122±29.65	0.00
1402+044	3	7864±1631	57.34±11.89	1.60±0.33	178.2±36.86	0.39±0.08	60.37±12.38	−0.08
1417+385	3	5622±879	17.15±2.68	1.12±0.18	27.8±4.37	0.74±0.14	25.01±4.55	−1.07
1502+106	3	5481±128	19.02±0.96	3.15±0.17	94.35±4.94	6.90±0.39	285.42±16.3	−2.50
1624+416	6	2818±1507	66.71±35.68	0.36±0.19	19.82±10.61	0.06±0.03	4.88±2.61	−4.12
1633+382	2,6	6499±29	25.63±3.79	12.97±1.73	318.55±41.58	5.29±1.06	176.38±3.32	−2.55
1638+398	2	9150±995	26.56±2.89	6.68±0.73	133.1±14.47	3.17±0.34	85.89±9.35	−0.01
1641+399	5	6710±1064	49.47±7.84	120.30±19.07	192.96±30.71	24.78±3.93	54.34±8.61	−0.07
1739+522	6	3445±942	12.53±3.43	8.52±2.33	128.87±35.24	10.55±2.39	219.87±50.05	−2.87
1758+388	2	6744±733	27.36±2.97	9.33±1.01	368.74±39.92	4.51±0.42	245.26±22.79	−0.02
1845+797	5	9135±210	92.48±18.70	284.65±37.12	3.65±0.48	69.00±2.19	1.26±0.04	−6.95
2126−158	2	5959±603	17.62±1.78	5.84±0.59	1022.33±103.28	3.84±0.42	960.32±104.78	−4.34
2128−123	5	8191±977	56.57±6.75	303.50±36.21	466.65±55.57	65.86±7.86	142.65±17.01	0.00
2134+004	1	7418±850	24.19±2.77	18.26±2.09	794.82±90.77	9.83±0.75	603.64±46.18	−0.89
2145+067	5	6423±638	32.44±3.22	69.59±6.91	663.85±65.91	24.01±2.68	327.08±36.52	4.83
2201+315	5	7939±790	21.92±2.18	229.40±22.83	165.8±16.51	132.43±10.19	140.86±10.88	−0.01
2216−038	5	8209±646	34.05±1.55	42.96±1.94	355.1±15.78	13.27±0.67	158.18±7.6	−3.18

TABLE 11 (CONTINUED)

		C IV (BC)				Continuum 1350 Å		
Name	Ref[a]	FWHM ($km\,s^{-1}$)	EW (Å)	Flux[b]	$L_{C\,IV}$ (10^{42} $erg\,s^{-1}$)	Flux[c]	λL_{1350} (10^{44} $erg\,s^{-1}$)	Spectral index[d]
2230+114	5	5990±403	20.96±1.41	25.94±1.74	255.71±17.18	13.40±1.11	188.01±15.57	−0.06
2243−123	5	7231±899	45.46±5.65	135.80±16.89	332.78±41.35	35.66±4.43	122.17±15.16	0.00
2251+158	5	7875±182	17.56±6.39	31.01±2.82	250.01±22.81	18.53±5.66	217.32±66.45	0.00
2351+456	6	5996±706	86.61±10.20	1.25±0.15	89.38±10.51	0.22±0.03	23.78±2.80	−4.49

[a]Spectrum reference: 1=OAGH; 2=OAN-SPM; 3=*SDSS* (Sloan Digital Sky Survey); 4=Marziani et al. (2003a); 5=*HST-FOS* (Hubble Space Telescope) y 6=Lawrence et al. (1996). If more spectra were available, the values are averaged and the error is the standard deviation.
[b]Flux in units of 10^{-15} $erg\,s^{-1}\,cm^{-2}$.
[c]Flux density in units of 10^{-16} $erg\,s^{-1}\,cm^{-2}\,Å^{-1}$.
[d]Spectral index for the local continuum.

REFERENCES

Arshakian, T. G., Chavushyan, V. H., Ros, E., Kadler, M., & Zensus, J. A. 2005, Memorie della Societa Astronomica Italiana, 76, 35

Arshakian, T. G., León-Tavares, J., Boettcher, M., Torrealba, J., Chavushyan, V. H., Lister, M. L., Ros, E., & Zensus, J. A. 2011, ArXiv e-prints (1104.4946)

Arshakian, T. G., León-Tavares, J., Lobanov, A. P., Chavushyan, V. H., Popovic, L., Shapovalova, A. I., Burenkov, A., & Zensus, J. A. 2008, Memorie della Societa Astronomica Italiana, 79, 1022

Arshakian, T. G., León-Tavares, J., Lobanov, A. P., Chavushyan, V. H., Shapovalova, A. I., Burenkov, A. N., & Zensus, J. A. 2010a, MNRAS, 401, 1231

Arshakian, T. G., Torrealba, J., Chavushyan, V. H., Ros, E., Lister, M. L., Cruz-González, I., & Zensus, J. A. 2010b, A&A, 520, A62

Brotherton, M. S., Tran, H. D., Becker, R. H., Gregg, M. D., Laurent-Muehleisen, S. A., & White, R. L. 2001, ApJ, 546, 775

Collin, S. & Joly, M. 2000, New Astronomy Reviews, 44, 531

Grandi, S. A. 1981, ApJ, 251, 451

Greenstein, J. L. & Schmidt, M. 1964, ApJ, 140, 1

Hough, D. H., Vermeulen, R. C., Readhead, A. C. S., Cross, L. L., Barth, E. L., Yu, L. H., Beyer, P. J., & Phifer, E. M. 2002, AJ, 123, 1258

Hovatta, T., Tammi, J., Tornikoski, M., Valtaoja, E., Torrealba, J., Chavushyan, V., Arshakian, T. G., & Cruz-Gonzales, I. 2010, in ASPC, Vol. 427, Accretion and Ejection in AGN: a Global View, ed. L. Maraschi, G. Ghisellini, R. Della Ceca, & F. Tavecchio, 34

Howarth, I. D. 1983, MNRAS, 203, 301

Joly, M. 1987, A&A, 184, 33

Kellermann, K. I., Lister, M. L., Homan, D. C., Vermeulen, R. C., Cohen, M. H., Ros, E., Kadler, M., Zensus, J. A., & Kovalev, Y. Y. 2004, ApJ, 609, 539

Kellermann, K. I., Vermeulen, R. C., Zensus, J. A., & Cohen, M. H. 1998, AJ, 115, 1295

Kovalev, Y. A., Kovalev, Y. Y., & Nizhelsky, N. A. 2000, in Astrophysical Phenomena Revealed by Space VLBI, ed. H. Hirabayashi, P. G. Edwards, & D. W. Murphy, 193

Kovalev, Y. Y., Kellermann, K. I., Lister, M. L., Homan, D. C., Vermeulen, R. C., Cohen, M. H., Ros, E., Kadler, M., Lobanov, A. P., Zensus, J. A., Kardashev, N. S., Gurvits, L. I., Aller, M. F., & Aller, H. D. 2005, AJ, 130, 2473

Kovalev, Y. Y., Nizhelsky, N. A., Kovalev, Y. A., Berlin, A. B., Zhekanis, G. V., Mingaliev, M. G., & Bogdantsov, A. V. 1999, A&AS, 139, 545

Kuraszkiewicz, J. K., Green, P. J., Forster, K., Aldcroft, T. L., Evans, I. N., & Koratkar, A. 2002, ApJS, 143, 257

Lawrence, C. R., Zucker, J. R., Readhead, A. C. S., Unwin, S. C., Pearson, T. J., & Xu, W. 1996, ApJS, 107, 541

León-Tavares, J., Lobanov, A. P., Chavushyan, V. H., Arshakian, T. G., Doroshenko, V. T., Sergeev, S. G., Efimov, Y. S., & Nazarov, S. V. 2010, ApJ, 715, 355

Lister, M. L., Cohen, M. H., Homan, D. C., Kadler, M., Kellermann, K. I., Kovalev, Y. Y., Ros, E., Savolainen, T., & Zensus, J. A. 2009, AJ, 138, 1874

Lister, M. L. & Homan, D. C. 2005, AJ, 130, 1389

Lister, M. L. & Smith, P. S. 2000, ApJ, 541, 66

Marziani, P., Sulentic, J. W., Zamanov, R., Calvani, M., Dultzin-Hacyan, D., Bachev, R., & Zwitter, T. 2003a, ApJS, 145, 199

Marziani, P., Zamanov, R. K., Sulentic, J. W., & Calvani, M. 2003b, MNRAS, 345, 1133
Massey, P., Strobel, K., Barnes, J. V., & Anderson, E. 1988, ApJ, 328, 315
McLure, R. J. & Dunlop, J. S. 2004, MNRAS, 352, 1390
Oke, J. B. 1990, AJ, 99, 1621
Osterbrock, D. E. 1977, ApJ, 215, 733
—. 1989, Astrophysics of gaseous nebulae and active galactic nuclei (Research supported by the University of California, John Simon Guggenheim Memorial Foundation, University of Minnesota, et al. Mill Valley, CA, University Science Books, 1989, 422)
Pen, U.-L. 1999, ApJS, 120, 49
Phillips, M. M. 1978, ApJS, 38, 187
Rokaki, E., Lawrence, A., Economou, F., & Mastichiadis, A. 2003, MNRAS, 340, 1298
Schlegel, D. J., Finkbeiner, D. P., & Davis, M. 1998, ApJ, 500, 525
Schmidt, M. & Green, R. F. 1983, ApJ, 269, 352
Schuster, W. J. & Parrao, L. 2001, RMxAA, 37, 187
Torrealba, J. 2010, PhD thesis, IA–UNAM, México
Torrealba, J., Arshakian, T. G., Chavushyan, V., & Cruz-Gonzalez, I. 2011, ArXiv e-prints (1104.2092)
Torrealba, J., Chavushyan, V. H., Arshakian, T. G., Cruz-González, I., Ros, E., Zensus, J. A., Bertone, E., & Rosa-González, D. 2008, in RMxAC, Vol. 32, 48
Veron, P., Lindblad, P. O., Zuiderwijk, E. J., Veron, M. P., & Adam, G. 1980, A&A, 87, 245
Véron-Cetty, M.-P., Joly, M., & Véron, P. 2004, A&A, 417, 515
Véron-Cetty, M.-P. & Véron, P. 2003, A&A, 412, 399
Vestergaard, M. & Peterson, B. M. 2006, ApJ, 641, 689
Vestergaard, M. & Wilkes, B. J. 2001, ApJS, 134, 1
Vestergaard, M., Wilkes, B. J., & Barthel, P. D. 2000, ApJL, 538, L103
Wills, B. J. & Browne, I. W. A. 1986, ApJ, 302, 56
Wills, B. J., Uomoto, A. K., Wills, D., & Netzer, H. 1980, ApJ, 237, 319
Zensus, J. A., Ros, E., Kellermann, K. I., Cohen, M. H., Vermeulen, R. C., & Kadler, M. 2002, AJ, 124, 662
Zhang, X., Dultzin-Hacyan, D., & Wang, T. 2007, RMxAA, 43, 101
Zhang, X.-G., Dultzin-Hacyan, D., & Wang, T.-G. 2006, MNRAS, 372, L5

T. G. Arshakian: Max-Planck/Institut für Radioastronomie, Auf dem Hügel 69, 53121 Bonn, Germany (tigar@mpifr-bonn.mpg.de)
E. Bertone, V. Chavushyan, D. Rosa-González and J. Torrealba: Instituto Nacional de Astrofísica Óptica y Electrónica, Apartado Postal 51 y 216, 72000 Puebla, Pue, México (ebertone,vahram,danrosa and cjanet@inaoep.mx)
I. Cruz-González: Instituto de Astronomía, Universidad Nacional Autónoma de México, Ciudad Universitaria, Apartado Postal 70–264, 04510, México D.F., México (irene@astroscu.unam.mx)